Title

Deciphering Nutritional Stress Responses via Knowledge-Enriched Transcriptomics for Microbial Engineering

Authors

Shin, Jongoh

Zielinski, Daniel C

Palsson, Bernhard O

Publication Date

2024-07-01

DOI

10.1016/j.ymben.2024.05.007

Metabolic Engineering 84 (2024) 34–47

Contents lists available at ScienceDirect

Metabolic Engineering

journal homepage: www.elsevier.com/locate/meteng

Deciphering nutritional stress responses via knowledge-enriched transcriptomics for microbial engineering

Jongoh Shin [a], Daniel C. Zielinski [a], Bernhard O. Palsson [a,b,c,*]

[a] Department of Bioengineering, University of California San Diego, La Jolla, CA, 92093, USA
[b] Novo Nordisk Foundation Center for Biosustainability, Technical University of Denmark, Lyngby, 2800, Denmark
[c] Department of Pediatrics, University of California, San Diego, La Jolla, CA, USA

ARTICLE INFO

Keywords:
Machine learning
Independent component analysis
Vibrio natriegens
iModulon
Nutritional response
Systems biology

ABSTRACT

Understanding diverse bacterial nutritional requirements and responses is foundational in microbial research and biotechnology. In this study, we employed knowledge-enriched transcriptomic analytics to decipher complex stress responses of *Vibrio natriegens* to supplied nutrients, aiming to enhance microbial engineering efforts. We computed 64 independently modulated gene sets that comprise a quantitative basis for transcriptome dynamics across a comprehensive transcriptomics dataset containing a broad array of nutrient conditions. Our approach led to the i) identification of novel transporter systems for diverse substrates, ii) a detailed understanding of how trace elements affect metabolism and growth, and iii) extensive characterization of nutrient-induced stress responses, including osmotic stress, low glycolytic flux, proteostasis, and altered protein expression. By clarifying the relationship between the acetate-associated regulon and glycolytic flux status of various nutrients, we have showcased its vital role in directing optimal carbon source selection. Our findings offer deep insights into the transcriptional landscape of bacterial nutrition and underscore its significance in tailoring strain engineering strategies, thereby facilitating the development of more efficient and robust microbial systems for biotechnological applications.

1. Introduction

Understanding microorganisms' nutritional requirements and responses is a critical component of microbiology, essential for their growth and functionality. The nutrient environment has been shown to significantly impact numerous cellular responses (Roszak and Colwell, 1987; Wang and Levin, 2009). These influences extend to the state of the transcriptional regulatory network (TRN), thereby affecting metabolic shifts (Balakrishnan et al., 2021; Basan et al., 2020; Erickson et al., 2017). Furthermore, these nutritional factors can trigger stringent response activation (Irving et al., 2021), alter pathogenicity (Eisenreich et al., 2010), influence antibiotic resistance (Martínez and Rojo, 2011), and even modify interspecies interactions (Bajic and Sanchez, 2020).

The emergence of genome-scale science, with available complete genome-wide profiling methods, allows the determination of the whole molecular state underlying an observed phenotypic state. In particular, after purification mRNA methods were established for bacteria (Croucher et al., 2009; Croucher and Thomson, 2010), a large number of transcriptomic profiles have become available in the public domain (Barrett et al., 2011; Leinonen et al., 2011). As transcriptomic compendia have grown, source signal extraction algorithms have been applied to identify independently modulated sets of genes (called iModulons). Independent component analysis (ICA), a machine learning method applied to transcriptomic compendia for various bacteria, has proved to be particularly effective (Saelens et al., 2018) for identifying quantitative and strain-specific TRNs (Rychel et al., 2021; Sastry et al., 2019). iModulons are big data analogs of regulons, and mapping of known regulatory and molecular biology information has knowledge-enriched the ICA signals, leading to a deep understanding of the modularization of TRNs and determination of their activity states (Lamoureux et al., 2023; Rychel et al., 2021).

We now have iModulons that 'measure' the activity states of 100s of cellular functions. These functions include metabolism, proteostasis, various stresses, two-component systems (Choudhary et al., 2020), antibiotic response (Rajput et al., 2022; Sastry et al., 2021a), adaptations to stresses (Rychel et al., 2023) and activation of latent phages (Poudel et al., 2020). The activity states of iModulons are a direct measure of the functional state of the TRN and what the cell is sensing

* Corresponding author. Department of Bioengineering, University of California San Diego, La Jolla, CA, 92093, USA.
E-mail address: palsson@ucsd.edu (B.O. Palsson).

https://doi.org/10.1016/j.ymben.2024.05.007
Received 7 February 2024; Received in revised form 27 March 2024; Accepted 28 May 2024
Available online 31 May 2024

and responding to in a particular environment. The abundance of transcriptomic data provides unprecedented opportunities to investigate and comprehend the intricate interactions across numerous organisms (Rychel et al., 2021). Notably, *Vibrio natriegens* (*Vn*), which has emerged as a novel chassis organism for molecular cloning and biotechnological applications (Thoma and Blombach, 2021), possesses the most extensive collection of single nutrient perturbation samples in minimal media among the ten species with available iModulon database. This collection spans a diverse range of substrates and stress conditions (Supplementary Figs. 1a and b). This extensive dataset enables a thorough investigation of cellular responses to various nutrient perturbations.

Here, by utilizing a comprehensive transcriptomic compendium for *Vn* under diverse nutrient conditions, we delve into the activity states of iModulons to decode the bacterium's responses to varying nutritional landscapes. Our investigation transcends traditional growth-centric approaches, offering a holistic view of the interplay between nutrient environments and the TRN. The insights gained deepen our understanding of microbial nutrition and stress responses and lay the groundwork for leveraging this knowledge in microbial research and biotechnology, guiding nutrient selection and informing genome engineering strategies.

2. Results

2.1. Modularization of the transcriptome to evaluate cellular responses to nutrients

Investigating *Vn*'s cellular responses to media composition changes, we focus on iModulons related to carbon utilization, trace elements, stress responses, and uncharacterized iModulons to establish a comprehensive framework for evaluating the effects of various nutrients on cellular processes (Fig. 1a).

We expanded the previous natPRECISE104 database (Shin et al., 2023) to natPRECISE148 by adding samples from the use of diverse substrates and stress conditions and analyzed using an ICA pipeline (Sastry et al., 2021b), resulting in 64 iModulons that enhance our insights into bacterial responses to nutritional and stress factors (**Supplementary Note** and Supplementary Fig. 1). Each iModulon was assigned to one of 11 functional groups, providing a systems-level perspective (Fig. 1b and Supplementary Fig. 1h). Comparing the 64 iModulons generated in this study with the 45 iModulons from our previous work (Shin et al., 2023), we found a substantial overlap, with 84% of the previous iModulons (38 out of 45) showing a significant correlation (Pearson's $R > 0.5$, P-value <0.0001) with the newly identified ones. This overlap effectively maps previously characterized regulatory signals to our latest findings (Supplementary Figs. 2a and b). This overlap suggests that the TRN structure remains robust to adding new data (Sastry et al., 2019). Despite its relatively small size compared to transcriptomic compendium for other bacterial species (Supplementary Fig. 1a), natPRECISE148 effectively captures unique catabolic iModulons (Supplementary Figs. 2c,d,e). The updated natPRECISE148 compendium reveals an increase in most iModulon categories, including eight new catabolic processes, four stress responses, four element homeostasis, two amino acid biosynthesis, two nitrogen and energy responses, and two natural competence, demonstrating comprehensive coverage of responses to changes in media composition (Supplementary Fig. 2a).

Using these 64 iModulons, this study covers a spectrum of transcriptional responses to diverse nutrient conditions (Fig. 1a). Our study covers various aspects of *Vn* nutrition, including nutrient uptake and catabolism, the involvement of metal ions as cofactors, their influence on protein synthesis and cell growth, and an array of specific stress responses. These stress responses include osmolarity and oxidative stress, challenges related to low glycolytic flux, and the activation of prophage genes. Condition-dependent iModulon activity levels allow us to decode intricate nutrient-cell response interactions and associated regulatory mechanisms.

2.2. Transcriptomic responses to substrates reveal TTT- and TRAP-related functions

We analyzed 15 substrate utilization iModulons in *Vn* across 21 substrates (Fig. 2a). Most iModulons were activated under their specific growth condition (the highlighted boxes with a thick green border, Fig. 2a). Additionally, multiple substrates activated unexpected iModulons.

Notably, the GalR and AGL iModulons, related to galactose and glycogen catabolism, showed a correlation (Pearson's $R = 0.62$, P-value <0.0001), indicating potential co-regulation (Fig. 2b and Supplementary Fig. 3a). Among the seven putative transcription factors, the one most strongly correlated with these iModulons is PN96_RS22690 (Pearson's $R = 0.69$, P-value <0.0001) suggesting that it could potentially regulate AGL iModulons (Supplementary Fig. 3b).

These experiments identified the TTT (Transporters and Tripartite Tricarboxylate Transporters) and TRAP (Tripartite ATP-Independent Periplasmic) iModulons. These systems, transporting small organic molecules via ion-electrochemical gradients (Mulligan et al., 2011; Rosa et al., 2018), exhibit varied substrate specificities (Herrou et al., 2007; Rosa et al., 2018; Rucktooa et al., 2007). Despite their distinct functional annotations, they share a common structural configuration for substrate binding, involving small (*tctC* for TTT iM; *dctP* for TRAP iM; RS19570 for GntR iM) and large subunits (*tctA* and *tctB* for TTT iM; *dctM* and *dctQ* for TRAP iM; RS19560 and RS19565 for GntR iM) that form the transmembrane channel (Fig. 2c and d). The substrate-binding protein component, which moves freely within the periplasm, is responsible for varied substrate binding and its delivery to the transmembrane components, enabling efficient transport across the membrane using sodium ion gradients.

The GntR iModulon also contains other TRAP genes with varying amino acid similarities (Fig. 2d). Interestingly, the TTT and TRAP iModulons are highly activated under growth on more than eight substrates, suggesting their pleiotropic role in the uptake of a broad range of substrates (Fig. 2a).

The TTT and TRAP iModulons, unique to *Vn* (Supplementary Fig. 2d), were further investigated alongside uncharacterized transporters in the GalR and Rhamnose iModulons. Comparing growth rates of knockout (KO) and WT (wild-type) strains revealed their roles in carbon utilization (Fig. 2e and Supplementary Fig. 3c). KO strains of TTT and TRAP iModulons exhibited significantly diminished growth rates (<0.85-fold, P-value <0.031) under four and seven carbon conditions, respectively. These findings suggest that the TTT and TRAP iModulons play a role in the uptake of certain carbon sources.

Interestingly, the deletion of TTT and TRAP iModulons resulted in not only decreased growth rates under certain conditions, but also enhanced growth with specific carbon sources such as trehalose, glycogen, arabinose, glucose, and GlcNAc (Fig. 2e). Given the constant expression of these transporters under the specified conditions (Supplementary Fig. 4a), this dual effect suggests that while these iModulons are important for the transportation of diverse substrates, their activity can occasionally impose an energetic burden, possibly by disrupting the optimal sodium ion gradient (Coppens et al., 2023). The alteration of this gradient, which is crucial for efficient ATP synthesis, highlights the complex relationship between transporter activity, ion homeostasis, and metabolic efficiency in *Vn*.

The KO strains of GntR and TRAP iModulons demonstrated distinct nutrient impacts, excluding fumarate, highlighting the substrate specificity differences between these two TRAP genes (Fig. 2e). Deletion of uncharacterized transporter genes (RS09130–RS09145) in the GalR iModulon led to a significant decrease in growth rate (<0.44-fold; P-value <0.00015) under galactose and cellobiose, further emphasizing the role of GalR iModulon in cellobiose utilization. Notably, rhamnose utilization highly depended on the uncharacterized transporter (RS17440) in the Rhamnose iModulon and on both TTT and TRAP iModulons. We further corroborated that the growth rates did not

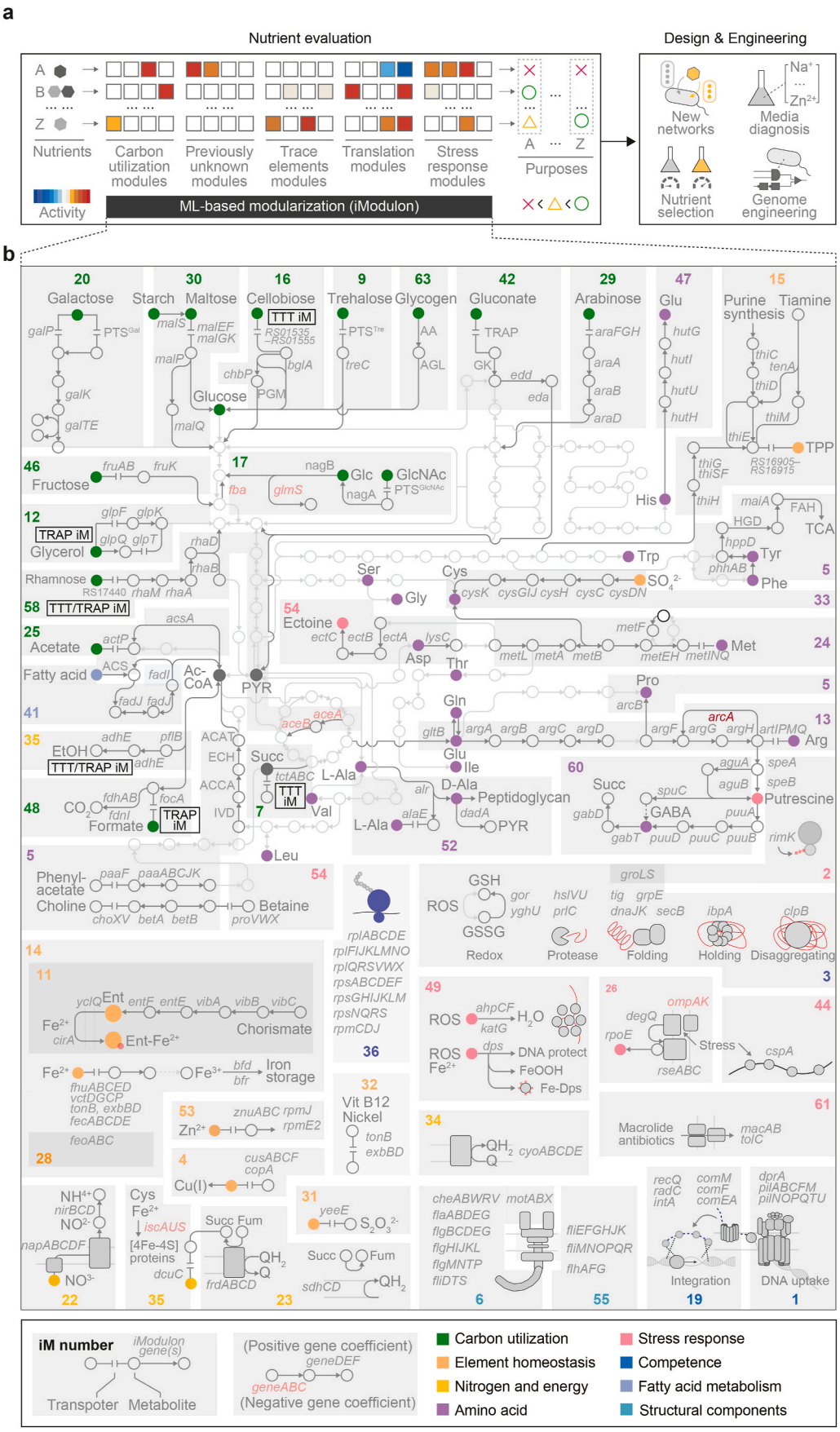

(caption on next page)

Fig. 1. Determining bacterial nutrition through deep transcriptome analysis. (a) The conceptual framework of this study. A matrix of detailed stress and nutrient transcriptomic responses can be evaluated for a large number of nutrient perturbations. The individual responses are characterized by the condition-dependent activity level of independently modulated sets of genes called iModulons. (b) Comprehensive map of the 46 iModulons identified using the natPRECISE148 compendium. Each iModulon number is represented with gene names enclosed in a gray box, indicating their association with a transcriptional regulator or cellular function. If the removal of TTT and TRAP significantly influences the growth rate under a specific carbon source (Fig. 2e), the corresponding TTT and/or TRAP iModulons are indicated in each respective carbon uptake pathway with a box. The shades of gray represent the genes contained in each iModulon and are darker when the genes in each iModulon overlap (e.g., Enterobactin iM). For detailed information on each iModulon number, please explore further on the iModulonDB website (https://www.imodulondb.org/) (Rychel et al., 2021). This visualization excludes certain iModulons for clarity, namely three categorized as Null, nine as Uncharacterized, two as Prophage, as well as the specific iModulons Biofilm, FNR, HapR, and PhrR.

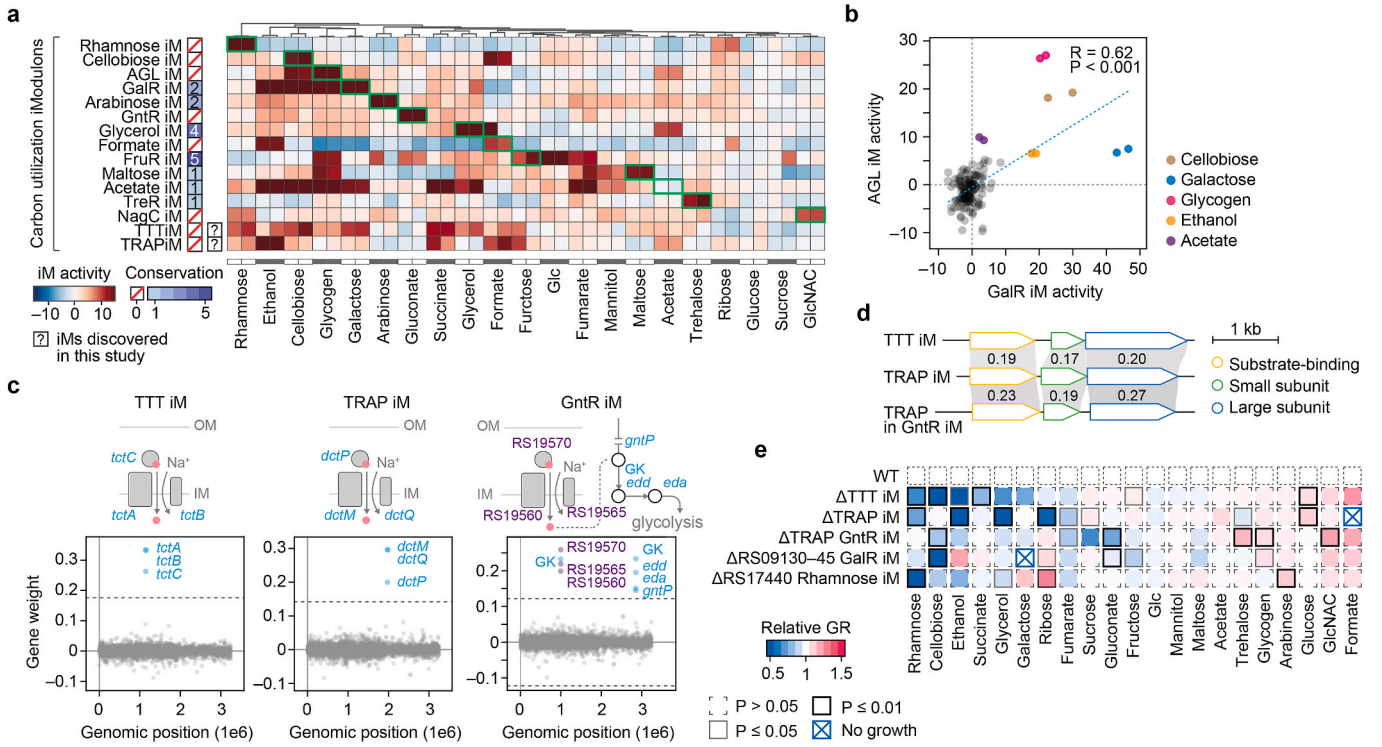

Fig. 2. Transcriptomic responses of *V. natriegens* to commonly used substrates. (a) The activity of 15 identified transcriptomic responses (rows) to various carbon sources (columns). The conservation of these iModulons was determined by comparing them with iModulons from other species (Supplementary Fig. 2d). Green boxes highlight the anticipated pairing of a substrate with its primary iModulon counterpart. The TTT and TRAP iModulons were previously unknown and discovered in this study. (b) Relationship between the activity levels of the AGL and GalR iModulons, representing galactose and glycogen catabolism, respectively. The Pearson's correlation coefficient (R) and the corresponding *P*-values are shown. (c) iModulon gene composition, described through gene weightings for the TTT, TRAP, and GntT iModulons and their genome position. The horizontal dashed lines indicate a cut-off threshold for gene weights. OM, outer membrane; IM, inner membrane. (d) Comparison between the TTT and TRAP iModulons within other TRAP genes in GntR iModulon. Connections between homologous genes are gray, with percentage sequence identity noted on the connecting lines. (e) Evaluation of the function of TTT iModulon, TRAP iModulon, and unknown transporters. To determine their role in growth, all genes within the TTT and TRAP iModulons, as well as selected gene members of the GntR, GalR, and Rhamnose iModulons, were deleted as detailed in Supplementary Fig. 3c. Each growth condition utilized a 15 mM concentration of the respective carbon source in M9Na minimal medium, with the exception of ethanol and formate conditions. Due to the inability of the wild-type (WT) strains to grow in the M9Na medium with the same carbon source concentration in ethanol and formate conditions, we instead used 1% wt/vol ethanol in M9Na and 40 g/L of sodium formate in LBv2. These conditions were consistent with those used in RNA-Seq generation conditions (Tian et al., 2023). The specific growth rates of these strains under various carbon conditions were measured, and the functions of deleted genes were inferred from the average relative growth rate (Relative GR) compared to the WT strain.

significantly deviate from those of the WT strain (0.91–1.34-folds, *P*-value >0.05) by supplementing each mutant with the expression of the deleted genes on a plasmid, as depicted in Supplementary Fig. 4b. The only exception to this was the ΔTRAP GntR iM strain (0.87-fold, *P*-value = 0.00017) under gluconate conditions. While our study provides insights into certain functions of these transporters, further extensive research is necessary to fully understand the unique mechanisms and roles of uncharacterized transporters within the GalR iModulon and Rhamnose iModulon.

Thus, iModularization of transcriptomic responses showed expected primary catabolic responses, revealed novel pleiotropic uptake mechanisms, and showed substrate-specific activation of several cellular processes. These substrate-specific responses were further delineated in the next section.

2.3. *iModulon activities reveal interactions of trace elements with substrates*

We examined the influence of trace elements in the medium on iModulon activity using various substrates in M9Na media, formulated without any supplementary trace element solutions. This approach revealed the significance of specific trace elements with specific substrates. Among seven iModulons associated with trace elements homeostasis (rows in Fig. 3a), the Zur iModulon, associated with Zn^{2+} transport, showed notable activation on many substrates, such as fructose and GlcNAc. In the assessment of trace element response, we noted distinct activities in the Zur and Fur2 iModulons across different replicates, particularly evident with substrates such as fructose and GlcNAc (Fig. 3a). These variations may reflect rapid transcriptional responses to

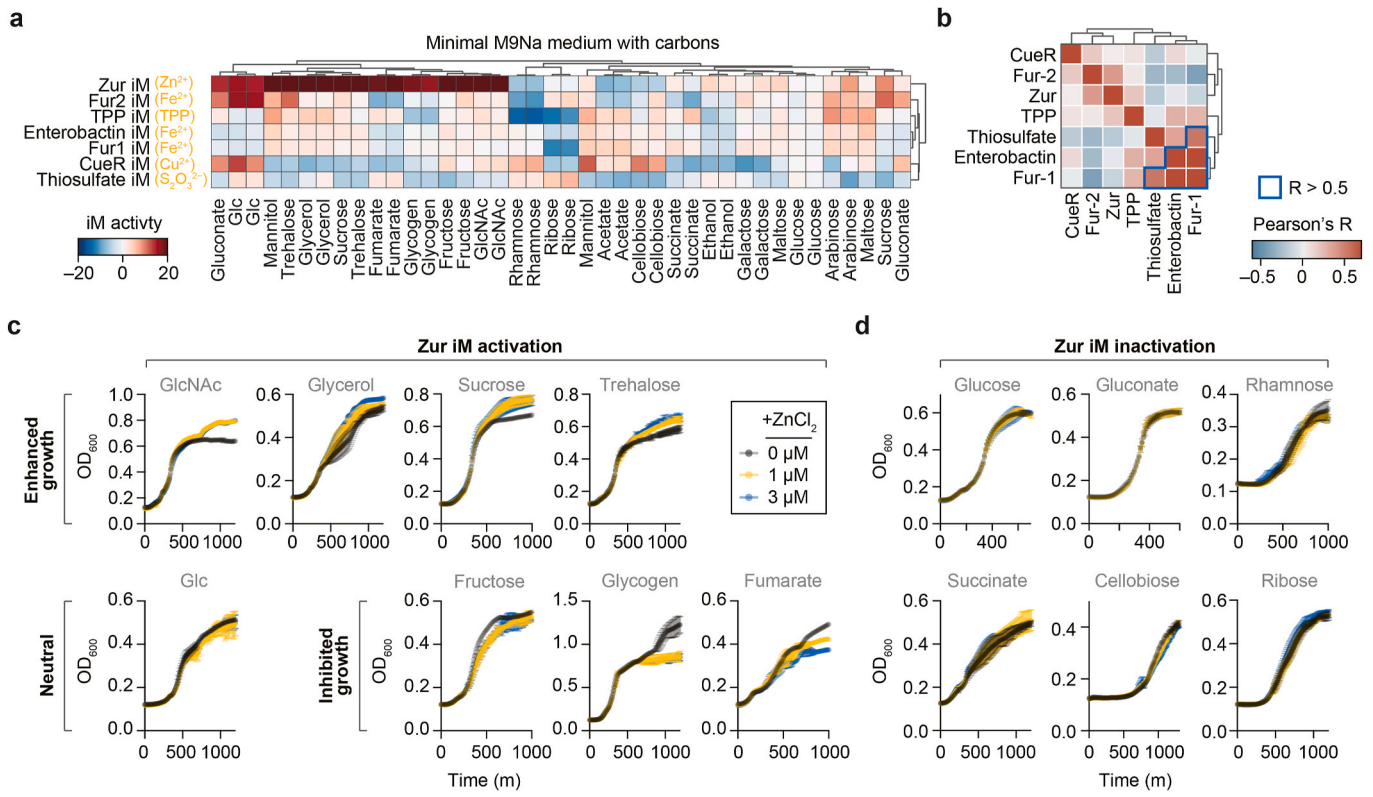

Fig. 3. Trace-element-related iModulon activity changes and cell growth variations across different substrates. (a) The activity of seven element homeostasis iModulons (rows) under various nutrient conditions (columns). (b) Activity correlation among the seven iModulons. (c, d) Growth profiles in various carbon conditions with $ZnCl_2$ treatment. For this, (c) 8 carbon sources known to induce Zur iModulon and (d) 6 carbon sources that do not induce Zur iModulon were utilized. Each condition uses a 15 mM concentration of the respective carbon source in M9Na minimal media. Data are presented as mean ± SD from four biologically independent samples.

the minimal trace-element concentrations present in the M9Na medium, a phenomenon consistent with the swift bacterial adaptation to fluctuations in metal ion availability (Miano et al., 2023).

Further analysis showed correlations between the seven iModulons (Fig. 3b). The Zur iModulon exhibited low correlation with the other six (Pearson's R < 0.37, *P*-value <0.0001). A strong correlation (Pearson's R = 0.80, *P*-value <0.0001) was observed between the Enterobactin and the Fur-1 iModulons, which was anticipated due to the overlap in their gene membership (Fig. 1b). Moreover, the Fur-1 iModulon showed a moderate correlation (Pearson's R = 0.53, *P*-value <0.0001) with the Thiosulfate iModulon activity. This indicates that Fur regulation may also affect thiosulfate uptake, creating a link between iron homeostasis and sulfur metabolism.

After supplementing M9Na media with $ZnCl_2$ at concentrations of 0, 1, and 3 μM—a typical range for trace element solutions (Soma et al., 2023) —we observed the effects on both substrates that activate the Zur iModulon and those that do not, assessing changes in growth rate. This approach revealed Zur iModulon activation's relationship with zinc ion levels, clarifying Zn^{2+} regulation under various growth conditions (Fig. 3c and d). This result indicates Zur iModulon's key role in Zn^{+2} regulation under these growth conditions. The growth responses to zinc supplementation were categorized as enhanced, neutral, and inhibited. Interestingly, significant improvements in growth rate (*P*-value <0.0195, excepting for trehalose) and maximum OD_{600} (*P*-value <0.041) were observed in GlcNAc, glycerol, sucrose, and trehalose conditions (Fig. 3c and Supplementary Fig. 3d). This enhancement indicates a Zn^{2+} dependency in pathways, such as GlcNAc catabolism involving the zinc-dependent NagA enzyme (Ferreira et al., 2006), contrasting with the non-zinc-dependent NagB enzyme, showing neutral growth response. Similar Zn^2 dependencies in glycerol (Ruzheinikov et al., 2001) and trehalose (Schothorst et al., 2017) catabolic enzymes in other species suggest a comparable requirement for *Vn* (Supplementary Fig. 3e).

Conversely, Zn^{2+} addition inhibited growth in fructose, glycogen, and fumarate conditions, evidenced by a decrease in growth rate (fructose, *P*-value $<2.1 \times 10^{-5}$) or maximum OD_{600} values (glycogen and fumarate, *P*-value $<3.4 \times 10^{-4}$) (Fig. 3c and Supplementary Fig. 3f). This inhibition suggests that Zn^{2+} negatively affected enzymes such as fructose kinase (Nocek et al., 2011) and glycogen debranching pullulanase (Asha et al., 2013; Bertoldo et al., 1999; Niehaus et al., 2000; Wangpaiboon et al., 2023; Wei et al., 2015). Furthermore, the identification of a putative inorganic ion transporter within the Zur iModulon (Supplementary Fig. 3g), a feature not observed in zinc-related iModulons in other species (Supplementary Fig. 3h), suggests a dual functionality in both zinc uptake and export, similar to that observed in *Salmonella* (Osman et al., 2017). In the *Pseudomonas putida* iModulon database (Lim et al., 2022; Rychel et al., 2021), a deactivation of Zur iModulon under the fructose indicates a potential Zn^{2+}-mediated regulatory requirement for the FruR iModulon's activities (Nocek et al., 2011).

Thus, iModulon analysis related to trace elements highlights the critical influence of trace elements in affecting iModulon activity and impacting bacterial growth across different substrates. Trace elemental composition of media may thus need alteration depending on the substrate for optimal and stress free growth.

2.4. *iModulon activity suggests an impact of nutrients on membrane and prophage-related stresses*

The expansion of the natPRECISE148 database, which includes RNA-Seq stress conditions such as temperature (25 °C and 40 °C), oxidative stress (0–0.4 mM of H_2O_2 in WT and VN-ALE-1 strains), and osmolarity

stress (0–800 mM of NaCl), has facilitated the identification of previously undiscovered stress-related iModulons, such as CSP, OxyR, Low-osmolarity, and Ectoine iModulons (Supplementary Fig. 2b).

The CSP and OxyR iModulons are responsible for the expression of cold-shock proteins and genes including *dps*, *katG*, *ahpC*, and *ahpF* that comprise the *oxyR* regulon, respectively (Supplementary Fig. 5). The CSP iModulon is deactivated under the 40 °C temperature condition (Supplementary Fig. 5a). The OxyR iModulon shows significant activation as a result of a mutated oxyR in the VN-ALE-1 strain, as illustrated in Supplementary Fig. 5b. This strain has adaptively evolved under H_2O_2 conditions (Anand et al., 2020). Conversely, the weak OxyR iModulon activation in the WT strain under H_2O_2 conditions may indicate a potential reason for the susceptibility of *Vn* to oxidative stress (Oliver, 2010; Weinstock et al., 2016).

In relation to membrane-associated stress, we identified two unique osmolarity-related iModulons: the Low-osmolarity and the Ectoine iModulons, responsible for putrescine and ectoine synthesis, respectively (Supplementary Figs. 6a and b). The Low-osmolarity iModulon, enhancing membrane stability, activates under low salt conditions, whereas the Ectoine iModulon, an osmoprotectant, activates under high salt conditions (iModulon activity >30). KO strains for these iModulons, subjected to varied salt concentrations, revealed their crucial role in osmotic stress adaptation, as indicated by changes in growth rates (Supplementary Fig. 6c).

Based on these findings, we employed nine stress-related iModulons to categorize substrates as stress-free (SF) or stress-inducing (SI) (Fig. 4a). While SI substrates typically exhibited lower growth rates compared to SF substrates (<0.63-fold, *P*-value <0.0001), an exception was noted in a 'High' group—comprising glycogen, succinate, and ribose—which did not follow this trend, maintaining relatively higher growth rates (1.17-fold, *P*-value = 0.004) (Fig. 4b).

In addition, RpoE, Ribosome, and Chaperone iModulons responded to large changes in salt concentration (Supplementary Figs. 6d,e,f,g). Acetate and rhamnose notably induced these iModulons (Fig. 4a) due to

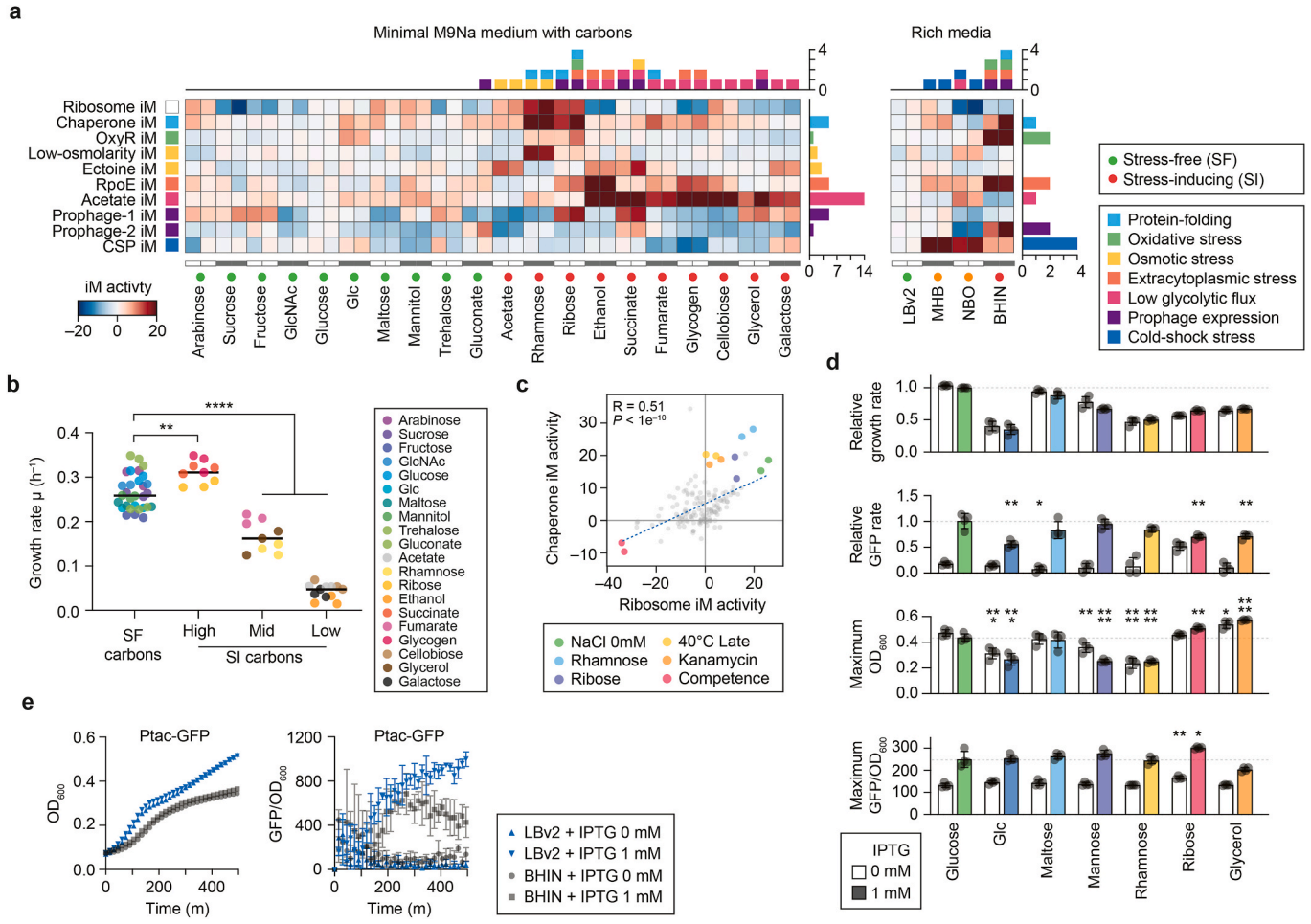

Fig. 4. Nutrients affect activity levels of Ribosome and nine stress-related iModulons and impact proteostasis. (a) The activity of nine stress-related and Ribosome iModulons (rows) under various substrates (columns). iModulon activities >10 in rich and minimal media are summarized in column and row plots associated with the heat map. Nutrients are classified as stress-free (SF) or stress-inducing (SI) based on the stress-iModulon activity that they induce. (b) Specific growth rate comparison between SF and SI substrates. SI carbons were classified into three groups based on their growth rate, ranging from "High" to "Low." Different color codes represent data from each substrate. WT *V. natriegens* were grown in 96-well plates, with OD_{600} measured using a Tecan Infinite 200Pro microplate reader. Each condition involved a 15 mM concentration of the respective carbon source in M9Na minimal media. The statistical significance was determined using Student's t-test (**$P < 0.01$; ****$P < 0.0001$). (c) Correlation between Chaperone and Ribosome iModulon activities. (d) Comparison of relative growth rate, relative GFP rates, maximum OD_{600}, and maximum cellular GFP signals (GFP/OD_{600}) in various carbon conditions. Each nutrient condition was compared to the glucose sample for relative growth and relative GFP rates. A dashed line represents the level of the glucose 1 mM IPTG sample. Data are presented as mean ± SD from four biological replicates. The statistical significance for each carbon condition, in comparison to the glucose sample with the same IPTG concentration, was determined using Student's t-test (*$P < 0.05$; **$P < 0.01$; ***$P < 0.001$; ****$P < 0.0001$), except for the relative growth rate graph. (e) Fluorescence and growth profile in LBv2 and BHIN Media. *V. natriegens* carrying Ptac-GFP plasmid grown in black/clear 96-well plates. GFP signal and OD_{600} measured. Cellular GFP signals (GFP/OD_{600}) were normalized to peak values. Mean ± SD from three independent samples.

the use of sodium acetate raising sodium levels in the medium (250 mM of M9Na +120 mM of Na^+ = 370 mM; Supplementary Fig. 6b) and rhamnose causing low salt stress through sodium ion-gradient dependent uptake via TTT and TRAP iModulons (Supplementary Fig. 6h). The RpoE iModulon's response to extracytoplasmic stress in glycogen or ethanol conditions aligns with other species' findings (Harty et al., 2019).

Furthermore, different substrates can activate Prophage-1 and Prophage-2 iModulons (iModulon activity >10, Fig. 4a and Supplementary Fig. 6i). This observation suggests that specific nutrients can elicit prophage activation, a process that can be both stressful and resource-intensive for bacteria (Carey et al., 2019; Derdouri et al., 2023).

These results reveal intricate relationships between substrates and stresses that they inflict on the host. These relationships can be detailed mechanistically in future studies.

2.5. Chaperone activation highlights protein expression and stress response dependence on media composition

We examined the activities of the Chaperone iModulon, and observed that cellular stress responses, including low salt conditions, stimulate its activity (Supplementary Figs. 6g and j). When we compared the activity of the Chaperone iModulon with that of 10 stress iModulons (Supplementary Fig. 6j), we found significant correlations with not only the Ribosome iModulon (Pearson's R < 0.51, *P*-value <0.0001) but also the low-osmolarity iModulon (Pearson's R < 0.35, *P*-value <0.0001). The correlation between Chaperone and Ribosome iModulon activities (Fig. 4c) indicated that certain conditions, such as rhamnose or ribose, might 1) challenge protein folding (Voth and Jakob, 2017), or 2) necessitate an increase in ribosome concentration, subsequently influencing the rate of protein synthesis in response to the intracellular nutritional state (Bosdriesz et al., 2015; Hidalgo et al., 2022).

To assess how nutrients affect proteostasis, we measured GFP protein expression across various substrates in M9Na media (Fig. 4d and Supplementary Fig. 7). Ribose showed a distinct pattern (Fig. 4d), with rhamnose activating Chaperone and Ribosome iModulons, this appeared to be an amplification due to the low-salt stress associated with rhamnose uptake (Fig. 4c and Supplementary Figs. 6e,f,g). Ribose, while not enhancing growth as rapidly as glucose (0.65-fold, *P*-value = 1.1×10^{-9}), showed the highest levels of relative fluorescence units (RFU; 1.9-fold, *P*-value = 7.7×10^{-6}) and RFU normalized by OD_{600} (1.2-fold, *P*-value = 0.027), indicating a significant increase in protein production within cells. Interestingly, ribose exhibited robust protein expression even without inducers (2.3-fold, *P*-value = 2.8×10^{-5}, compared to glucose) (Fig. 4d), suggesting that it may activate a stress response that enhances translation more effectively than other carbons. Therefore, choosing substrates activating Ribosome and Chaperone iModulons might enhance protein production.

Additionally, our analysis revealed that the complex media BHIN (Brain Heart Infusion + 1.5% wt/vol NaCl) triggered several stress iModulons (Fig. 4a). This led to lower growth rates (0.5-fold, *P*-value = 1.5×10^{-8}, Supplementary Fig. 6k), slower rates of RFU increase (0.7-fold, *P*-value = 0.048), and lower maximum RFU/OD_{600} levels (0.41-fold, *P*-value = 0.0005) versus LBv2 medium (Fig. 4e). These findings suggest that BHIN might not be ideal for *Vn* cultivation.

Thus, substrates can induce specific stresses, with substrate choice impacting translation and protein production. This shows that substrate selection is crucialin bacterial cultivation and strain development, influencing growth and protein synthesis efficiency.

2.6. Nutrients affect acetate iModulon activity that is associated with glycolytic flux

We observed striking behavior of the Acetate iModulon across various substrates (Fig. 2a and 4a), prompting a deeper analysis. The Acetate iModulon, involved in both carbon utilization and stress response, displayed patterns indicative of its involvement in low glycolytic flux states (Millard et al., 2023). This finding indicate the Acetate iModulon (Supplementary Fig. 8a) could be a biomarker for low flux glycolytic states (Fig. 5a).

In *Escherichia coli*, acetate metabolism involves phosphotransacetylase (Pta) and acetate kinase (Ack), with the acetate CoA-synthetase (AcsA) gene playing a pivotal role (Millard et al., 2021) (Fig. 5a). AcsA crucially converts acetate into acetyl-CoA, essential forthe acetate switch process. Similarly, the Acetate iModulon in *Vn* includes the Acs enzyme, the acetate symporter (ActP), acyl-CoA synthetase, methylisocitrate lyase, and eight additional proteins with functions to be elucidated. Bacteria typically excrete acetate when utilizing standard carbon sources, like sugars, then re-uptake it when depleted, particularly in the stationary phase (Wolfe, 2005) (Supplementary Fig. 8b). SF substrates that promote high glycolytic flux tend to lead to acetate secretion, as acetate inhibits both the glycolytic pathway and the TCA cycle (Millard et al., 2021). Conversely, poor carbon sources inducing low glycolytic flux activate the Acetate iModulon, facilitating acetate reuse or limiting secretion (Millard et al., 2023). For instance, *E. coli* growing on glycerol, a poor carbon source, employs a "carbon source foraging strategy", avoiding acetate production (Martínez-Gómez et al., 2012).

To further investigate this effect, we added 5 mM acetate (Millard et al., 2023) to various substrates in M9Na. This addition generally reduced growth rate (0.69–0.88-fold, *P*-value <0.0001) in SF carbon samples, except for glucosamine, but improved growth rate under SI conditions (1.15–5.51-fold, *P*-value = 0.0002) (Fig. 5b and Supplementary Fig. 8c). Rhamnose and ribose, not inducing the Acetate iModulon, exhibited expected growth patterns. KO studies of the Acetate iModulon gene (RS14410–RS14420) indicated improved growth rate in SF carbons (1.11–1.28-fold, *P*-value <0.0001, except for gluconate and glucosamine) but reduced growth rate in SI conditions (0–0.89-fold, *P*-value <0.0001, except for ribose and succinate) (Fig. 5c and Supplementary Fig. 8d). Notably, both acetate and, unexpectedly, galactose significantly depend on the Acetate iModulon (no growth with ΔAcetate iM, *P*-value <0.0001), underscoring its importance (Fig. 5d).

Despite the limited availability of single nutrient perturbation samples (Supplementary Fig. 1a), consistent patterns in the Acetate iModulon have been identified across species in the iModulonDB (Rychel et al., 2021). In the *Pseudomonas putida* iModulon database, certain carbon sources such as ferulate, citrate, coumarate, fructose, and serine, and specific genomic modifications (Bentley et al., 2020) were found to activate the starvation-related BkdR iModulon (Lim et al., 2022) along with the Acetate iModulon. The simultaneous activation suggests a significant correlation (Pearson's R = 0.57, *P*-value <0.001) between BkdR and Acetate iModulons (Supplementary Fig. 8e). Similarly, in *E. coli*, the Acetate iModulon is activated by carbon sources such as fructose, acetate, and glycerol, highlighting their limited role as general-use carbon sources without inducing acetate secretion (Chang et al., 1999; Farmer and Liao, 1997; Martínez-Gómez et al., 2012).

Furthermore, we identified a novel interaction between the TTT and TRAP iModulons and SI substrates. These iModulons were significantly activated under SI conditions (average 21.1-fold for TTT iModulon and 381.8-fold for TRAP iModulon, *P*-value <0.001) (Fig. 5e). Consequently, there is a correlation between Acetate iModulon activity and the TTT and TRAP iModulons (Fig. 5f). Comparisons revealed that the TRAP iModulon activation is growth phage-independent, unlike the TTT iModulon, and uncorrelate with the GntR iModulon's different TRAP genes (Fig. 5f). Overall, our findings provide insights into cells adaptation to poor carbon sources via the TTT/TRAP and Acetate iModulons (Supplementary Fig. 8f).

In summary, the Acetate iModulon's response to various nutrients reveals its importance as an indicator of low glycolytic flux, providing insights into bacterial metabolism and potential strategies for optimizing substrate utilization.

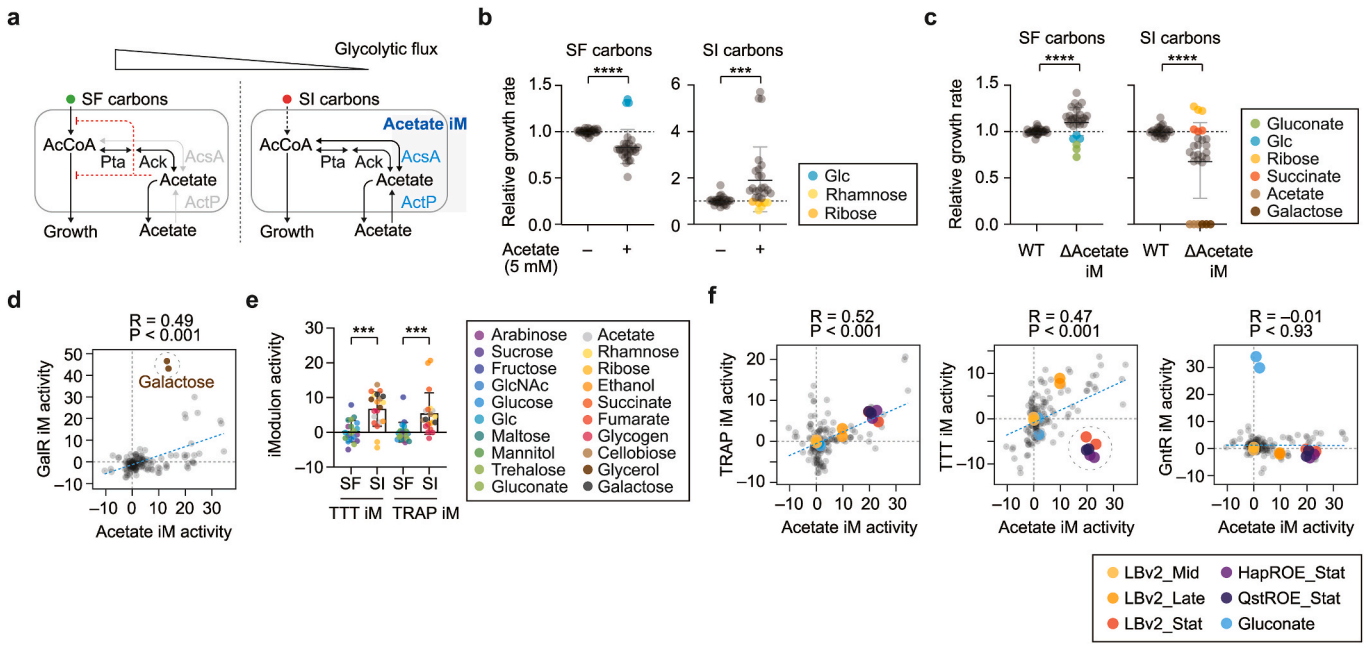

Fig. 5. Functions of the Acetate iModulon under low-glycolytic flux conditions. (a) Graphical summary depicting the function of the Acetate iModulon in central carbon metabolism at low glycolytic flux states. A red dashed line indicates acetate-induced inhibition of glycolysis and TCA cycle enzymes. Inspired by the previous study (Millard et al., 2023). (b, c) Analysis of (b) acetate supplementation and (c) Acetate iModulon gene deletion effects in stress-inducing (SI) and stress-free (SF) carbon conditions. Specific growth rates were measured following these modifications in SI and SF conditions, compared to control conditions (no acetate or WT strain). Statistical significance in SI and SF environments was evaluated using the two-tailed Mann-Whitney test (***$P < 0.001$; ****$P < 0.0001$). Color coding distinguishes specific carbon conditions, and detailed growth rate changes for each carbon source are provided in Supplementary Figs. 8c and d. (d) Correlation between Acetate and GalR iModulons' activities. Pearson's R (R) and *P*-value (P) are displayed. (e) TTT and TRAP iModulons' activity under SI and SF carbon conditions. Statistical significance was assessed using the two-tailed Wilcoxon matched-pairs signed rank test (***$P < 0.001$). (f) Interrelations among Acetate, TRAP, TTT, and GntR iModulons. Pearson's R (R) and *P*-value (P) are shown.

2.7. Enhancing growth on poor carbon sources via acetate iModulon boosting

Finally, we evaluated the potential use of the Acetate iModulon for strain engineering, aiming to elevate its activity without disrupting its natural regulation. This strategy aims to boost growth under most SI carbon sources (Fig. 6a), keeping the Acetate iModulon inactive under SF carbon conditions (Millard et al., 2021; Pinhal et al., 2019).

Implementing this strategy, we integrated a 'boost module' genetic circuit adjacent to the original Acetate iModulon genes in the genome (Fig. 6b and Supplementary Fig. 8g). This circuit included *araC* positioned after the original Acetate iModulon genes, tasked with repressing the *lacI* gene. This *lacI*, in turn, represses an additional set of Acetate iModulon genes within the boost module. Such a design amplifies the Acetate iModulon activity specifically under poor carbon source conditions. We engineered two strains, Boost-A and Boost-B, by integrating this booster module after the original Acetate iModulon genes. Boost-A included *acsA*, RS14450, and *acsP*, whereas Boost-B contained only the key enzyme *acsA*.

Our experiments revealed minimal growth differences between the control and the two booster strains under SF conditions, except for Boost-B in glucosamine and mannitol conditions. However, under SI carbon sources, the engineered strains exhibited significant growth enhancements, as evidenced by increased growth rates (1.1–2.4-fold, *P*-value <0.034) and shorter lag times (0.47–0.81-fold, *P*-value <0.005) in the Boost-A strain (Fig. 6c and d and Supplementary Fig. 8h), except for ribose which did not induce the Acetate iModulon. Thus, activating the Acetate iModulon can substantially improve the utilization of poor carbon sources, demonstrating the practical application of iModulon information from nutrient change experiments for optimization of cellular functions.

3. Discussion

How can modern genome-scale methods enhance our understanding of microbial responses to nutritional stress for strain engineering? This study used advanced modularization methods to analyze the bacterial transcriptome, revealing the activation state of various cellular processes in response to different nutrient states in *Vn*. These processes, which are independently modulated, include catabolism, trace elements use, proteostasis, phage activation, and various stress responses (Balakrishnan et al., 2021; Basan et al., 2020; Erickson et al., 2017).

Analyzing catabolic iModulon activity revealed pathways activated by different nutrients, unearthing new iModulons linked to substrate uptake. Notable are the pleiotropic TTT and TRAP iModulons (Mulligan et al., 2011; Rosa et al., 2018), important for metabolizing nine substrates such as rhamnose, cellobiose, and formate, underscoring their broad substrate utility in *Vn* (Thoma and Blombach, 2021). We also unraveled novel regulatory relationships and gene functions in catabolism, such as interactions within specific substrates such as cellobiose, galactose, and glycogen, especially regarding the GalR and AGL iModulons activities. Additionally, we observed interconnections among Acetate, TTT, and TRAP iModulons under conditions inducing low-glycolytic flux, enhancing our understanding of *Vn*'s metabolic adaptability.

iModulon analysis, mainly focusing on the Zur iModulon, illuminated the complex interplay between trace elements like Zn^{2+} and various substrates. This analysis highlights the intricate regulatory mechanisms that control trace elements such as Zn^{2+}, essential for bacterial metabolism and growth. Fine-tuning trace elements, as evidenced by the Zur iModulon activities, is shown to impact bacterial physiology substantially. This balancing includes influencing physiological activities (Soma et al., 2023), optimizing large-scale cultivation processes (Soini et al., 2008), regulating the expression of heterologous

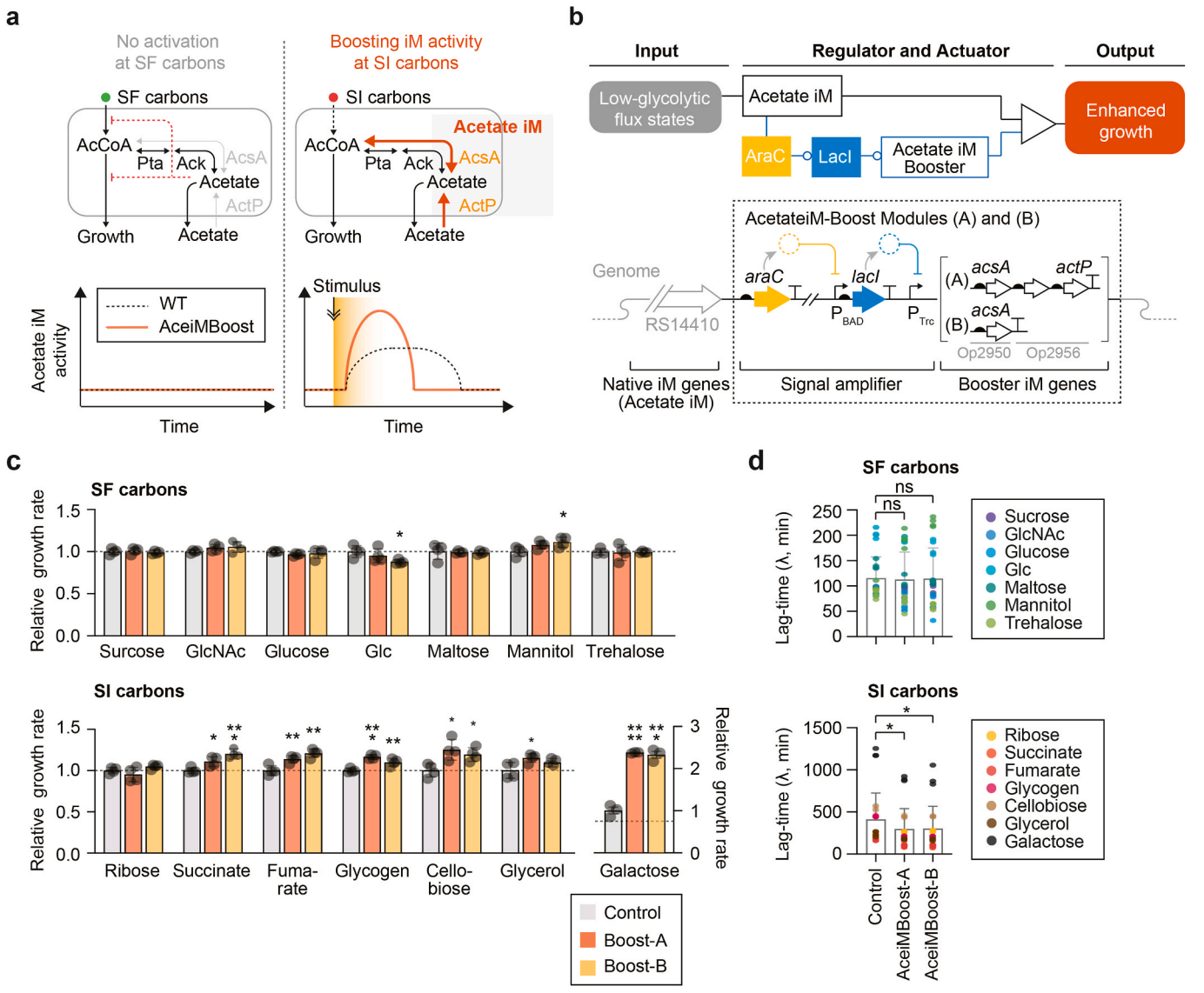

Fig. 6. Strain engineering with the Acetate iModulon. (a) Graphical overview of enhancing Acetate iModulon function with native regulation. AceiMBoost is activated in low glycolytic flux states to enhance the phenotype. (b) Schematic of the Acetate iModulon boosting circuit (top) and its genomic integration (bottom). AcetateiM-Boost modules (Boost-A and Boost-B) are integrated following the native acetate iModulon gene (RS14410). For simplicity, all constructs except *araC* and *araC*'s RBS are depicted on the same strand as *araC*, though actual integration is in the opposite direction. Boost-A contains two operons of the Acetate iModulon, while Boost-B includes the *acsA* gene with a terminator. (c, d) Changes in growth rate and lag-time due to the Acetate iModulon boosting module. Two Boost strains and a control strain were cultured in 15 mM carbon source in M9Na minimal media, with OD_{600} measured using a Tecan Infinite 200Pro microplate reader. (c) Relative growth rates compared to the control. (d) Lag times are compared to the control. Data are mean ± SD from three to four independent samples. Growth rate statistical significance was determined using Student's t-test (*$P < 0.05$; **$P < 0.01$; ***$P < 0.001$; ****$P < 0.0001$). Lag-time significance was assessed with the two-tailed Mann-Whitney test (*$P < 0.05$).

proteins (Rosano and Ceccarelli, 2014; Shang et al., 2023), affecting anaerobic metabolism (Stadtman, 2005), and enhancing biochemical production (Nimbalkar et al., 2018).

Stress-response iModulons analysis uncovers the diverse physiological challenges of different nutrients, moving beyond the traditional focus on carbon starvation (Kolb et al., 1993; You et al., 2013) and the stringent response (Irving et al., 2021; Zhu and Dai, 2023). We identified stress responses related to protein-folding, oxidative, extracytoplasmic, and osmotic stress. This broadened understanding illuminates how bacteria adapt to nutritional changes. Notably, stresses in commonly used BHIN media for *Vn* studies (Eagon, 1962; Hoffart et al., 2017; Xu et al., 2021), such as oxidative and extracytoplasmic stress, are linked to reduced growth rates and protein synthesis. The high- and low-osmolarity stresses due to sodium acetate and rhamnose usage illustrates the influence of carbon source types and their specific uptake mechanisms, particularly involving TTT and TRAP iModulons. These results reveal intricate relationships between substrates and the stresses they inflict on the host. Furthermore, activating the Acetate iModulon under certain conditions reveals insights into bacterial metabolic adjustments for low glycolytic flux (Millard et al., 2023).

This study highlights the utility of iModulon analysis in selecting optimal nutrient and guiding strain engineering. By analyzing iModulon activities, we can select nutrients tailored to specific experimental objectives. A notable example is ribose, which stands out for its potential to boost protein expression in *Vn*. Ribose is pivotal in maintaining intracellular redox balance and promoting efficient amino acid biosynthesis (Moritz et al., 2002; Sui et al., 2020). Its unique ability to activate Ribosome and Chaperone iModulons—without inducing the osmolarity stress responses observed with rhamnose—suggests a potential to increase heterologous protein production. Stress-free growth conditions

are crucial for understanding bacterial pathogenicity (Fang et al., 2016), metabolism (Jozefczuk et al., 2010), and antibiotic resistance (Dawan and Ahn, 2022). Also, the detailed insights provided by gene membership and iModulon activity dynamics across various conditions are invaluable for microbial engineering, such as using the Acetate iModulon to boost growth on poor carbon sources.

Taken together, this study underscores the pivotal role of knowledge-enriched transcriptomic analysis in deciphering the very intricate relationships between the state of cellular processes and the nutritional environment. This approach advances our knowledge of bacterial nutrition and paves the way for future innovations in microbial research, offering new possibilities for understanding and manipulating the state of fundamental cellular responses in bacteria.

4. Materials and methods

4.1. Bacterial strains and growth conditions

Bacterial strains, both utilized and generated for this study, are listed in Supplementary Table 1. This study used *Vibrio natriegens* ATCC 14048 (*Vn*) as the wild-type strain. Routine cultivation of *Vn* was conducted at 30 °C in LBv2 media (25 g/L LB Miller broth, 200 mM NaCl, 4.2 mM KCl, and 23.14 mM MgCl2), agitated at 180 RPM, or on LBv2 agar plates (LBv2 plus 1.5% wt/vol agar). Brain Heart Infusion broth with added NaCl (BHIN: 37 g/L, 1.5% wt/vol) served as a comparative medium to LBv2. For the construction of 44 RNA-Seq data, *Vn* strains were cultivated at 30 °C with agitation at 180 RPM. Unless stated otherwise, chemical reagents used for cell culture were sourced from Sigma-Aldrich (Burlington, MA). For additional RNA-Seq carbon samples, a range of carbon sources were added into M9Na medium (M9 minimal medium enriched with NaCl [42 mM Na_2HPO_4, 22 mM KH_2PO_4, 258.5 mM NaCl, 18.6 mM NH_4Cl, 2 mM $MgSO_4$, 0.1 mM $CaCl_2$]) at a uniform concentration of 1.0% wt/vol, including sodium acetate, cellobiose, glycogen, and rhamnose, consistent with previous data (Shin et al., 2023). Oxidative stress conditions in M9Na were induced by adding H_2O_2 (0 mM, 0.1 mM, 0.2 mM, and 0.4 mM) to WT and VN-ALE-1 strains, the latter being an evolved strain from adaptive laboratory evolution experiments under oxidative stress (Anand et al., 2020). Low- and high-temperature stress conditions were set in M9Na at 25 °C and 40 °C, respectively. Osmolarity stress conditions were established by varying NaCl concentrations (0, 200, 500, and 800 mM) in M9woNa (M9 medium without NaCl [42 mM Na_2HPO_4, 22 mM KH_2PO_4, 18.6 mM NH_4Cl, 2 mM $MgSO_4$, 0.1 mM $CaCl_2$]). When an antibiotic selection of *Vn* was required, the antibiotics were used at specified concentrations: 50 μg/mL carbenicillin (Carb), 10 μg/mL chloramphenicol (Cm), or 360 μg/mL spectinomycin (Spec). For plasmid cloning, NEB® 10-beta Competent *Escherichia coli* (New England BioLabs, Ipswich, MA) was cultivated aerobically at 37 °C in LB Miller broth (LB, #71753–6) with shaking at 180 RPM or on LB agar (LB with 1.5% wt/vol agar). When *E. coli* harbored a plasmid, appropriate antibiotics were used: 100 μg/mL ampicillin/carbenicillin, 25 μg/mL chloramphenicol, or 120 μg/mL spectinomycin.

4.2. RNA extraction and transcriptomic data generation

We produced a total of 44 new RNA-Seq datasets pertinent to carbon and stress-related conditions. For each of the 22 unique conditions, including various carbon sources (acetate, cellobiose, glycogen, and rhamnose), temperature stress (25 °C and 40 °C), oxidative stress (0, 0.1, 0.2, and 0.4 mM H_2O_2), and salt stress (0, 200, 500, and 800 mM NaCl), we obtained transcriptomic data from two biological replicates. The RNA extraction and library preparation procedures were in accordance with the protocol established in our prior study (Shin et al., 2023). Briefly, samples were centrifuged for 10 min at 5000×*g* at 4 °C, and the supernatant was removed. RNA was isolated from the harvested cells using the Quick-RNA Fungal/Bacterial Microprep Kit (Zymo Research, Irvine, CA), according to the manufacturer's guidelines. As previously described, ribosomal RNA and genomic DNA contaminants were eliminated from 1 μg total RNA using the RiboRid method (Choe et al., 2021; Shin et al., 2023). rRNA depletion was verified via the 4150 TapeStation System (Agilent, Santa Clara, CA) with High Sensitivity RNA ScreenTape. The rRNA-depleted RNA was then converted into libraries using the KAPA RNA HyperPrep kit (Roche, Basel, Switzerland) following the manufacturer's protocols. Library quality was assessed with the 4150 TapeStation System (Agilent) using D1000 ScreenTape, and quantification was done with the Qubit 2.0 Fluorometer (Thermo Fisher Scientific, Waltham, MA) using the Qubit dsDNA HS Assay Kit. Subsequently, the libraries were combined and sequenced using a 100 bp single-end protocol on the Illumina NovaSeq 6000 platform at the UC San Diego IGM Genomics Center.

4.3. Compilation of natPRECISE148 dataset

In this study, in addition to the 44 RNA-Seq datasets we generated, we also included 8 RNA-Seq samples from the NCBI Sequence Read Archive, accessed before March 1, 2023, using the fasterq-dump software from https://github.com/ncbi/sra-tools. This expanded our collection to a total of 52 RNA-Seq samples. For data processing and quality control prior to Independent Component Analysis (ICA), we followed the procedures outlined in the Modulome workflow, detailed at https://github.com/avsastry/modulome-workflow (Sastry et al., 2021b). Initially, raw read trimming was performed using Trim Galore, available at https://www.bioinformatics.babraham.ac.uk/projects/trim_galore/, and FastQC, found at https://www.bioinformatics.babraham.ac.uk/projects/fastqc/. The quality reads were then aligned to the *Vn* reference genome (GCA_001456255.1) (Lee et al., 2019) using Bowtie (Langmead et al., 2009). We converted the generated SAM files into BAM files using the sam2bam function of Samtools, available at http://www.htslib.org/. Gene read counts in each library were computed with RSeQC (Wang et al., 2012) and FeatureCounts (Liao et al., 2014). All quality control metrics were compiled using MultiQC at https://multiqc.info/(Ewels et al., 2016). To maintain high data quality, we excluded datasets that failed to meet any of the following FASTQC criteria: per_base_sequence_quality, per_sequence_quality_scores, per_base_n_content, and adapter_content. Samples with fewer than 400,000 reads mapped to coding sequences were also discarded. To minimize technical variability, samples were further filtered out based on three conditions: (a) deviation from the general expression pattern, as determined by hierarchical clustering, (b) weak correlation within biological replicates (R^2 less than 0.90), and (c) absence of a biological replicate, as detailed in Supplementary Figs. 1b and c. After thorough quality control, our final natPRECISE148 (natrigens Precision RNA-seq Expression Compendium for Independent Signal Exploration) contained 148 high-quality expression profiles: 104 from the previous natPRECISE104 database (Rychel et al., 2021; Shin et al., 2023), 42 generated in this study, and 2 expression profiles (Tian et al., 2023) derived from public databases. The read counts were then normalized and presented as log_2-transformed Transcripts per Million (log-TPM).

4.4. Independent component analysis (ICA)

We used the bioinformatics pipeline detailed in previous studies (Sastry et al., 2019, 2021b; Shin et al., 2023). ICA was utilized to decompose the transcriptomic data matrix (X, 4515 genes by 148 conditions) into two components (M and A, representing iModulons and their activities, respectively). We calculated independent components (ICs) through 100 iterations with the FastICA algorithm (Hyvärinen, 1999) and Scikit-Learn (Pedregosa et al., 2011) and then clustered these ICs using Scikit-Learn's DBSCAN (Ester and Sander, 1996) to determine robust ICs. The optimal dimension for ICs was ascertained iteratively (McConn et al., 2021), testing dimensions from 10 to 150 in steps of 10 as per (Sastry et al., 2019). The dimension of 140 was chosen based on

the consistency between the number of robust components and the final components at this dimension (Supplementary Fig. 1e). Consequently, we derived an M matrix with 64 robust iModulons and an A matrix detailing their activities across conditions. In the M matrix, each iModulon's gene weighting was determined, though most were insignificant. Significant iModulon genes were identified by setting optimal thresholds based on the D'Agostino K^2 test in Scikit-Learn, as delineated in previous studies (Sastry et al., 2019, 2021b; Shin et al., 2023). The process involved iteratively removing genes with the highest absolute weight until the remaining genes approximated a normal distribution (D'Agostino K^2 test statistic <500). The genes and weights removed at this point were deemed significant, setting the iModulon thresholds.

4.5. Functional characterization of iModulons

The functional characterization of iModulons was conducted as described in a previous study (Shin et al., 2023). Briefly, we utilized the Pymodulon tool (https://github.com/SBRG/pymodulon) to examine 64 identified iModulons. Our initial step involved augmenting the transcriptional regulatory network (TRN) to ascertain the functions of these iModulons, utilizing 931 TF-gene interactions previously identified (Shin et al., 2023). We inferred the transcription regulators for each iModulon using Fisher's Exact Test, applying a Benjamini-Hochberg correction to control the false discovery rate (FDR) below 10^{-5}. iModulons with significant overlap with the TRN were named according to the associated transcription factors (TFs). Furthermore, iModulon functions were deduced by gene annotation against the Kyoto Encyclopedia of Genes and Genomes (KEGG) (Kanehisa et al., 2017) and the Cluster of Orthologous Groups (COG) databases, utilizing the EggNOG mapper (Huerta-Cepas et al., 2019). KEGG modules with a statistically significant Benjamini-Hochberg corrected FDR of less than 10^{-2} (Fisher's Exact test) were noted. We obtained Uniprot IDs through the Uniprot ID mapper (UniProt Consortium, 2021) and sourced operon information from BioCyc (Karp et al., 2019). Additionally, Gene Ontology (GO) annotations were acquired from AmiGO2 (Gene Ontology Consortium, 2021). Each iModulon was then named based on its significantly enriched functional traits.

4.6. Optical density and fluorescence measurement

For flask culture experiments, the optical density (OD_{600}) at 600 nm of bacterial cultures was determined using the BioMate™ 3S Spectrophotometer (Thermo Fisher Scientific, Waltham, MA). Additionally, the optical density for bacterial cultures was measured at 600 nm using the Infinite 200 Pro Plate Reader (Tecan, Männedorf, Switzerland). The measurements were conducted in Flat Bottom 96-well plates, with each well containing 100 μl of culture. For experiments involving Green Fluorescent Protein (GFP), fluorescence and/or OD_{600} were assessed using the same plate reader. This was done at 485/515 nm excitation/emission wavelengths, utilizing Bio-One CELLSTAR μClear™ 96-well plates (Greiner, Kremsmünster, Austria). The plates were incubated at 30 °C with orbital shaking. Measurements of OD_{600} or fluorescence signals were recorded at 10 to 15-min intervals. Relative fluorescence units (RFU) were adjusted by deducting the corresponding blanks, specifically the medium both with and without molecules. For the analysis of growth dynamics and GFP expression, parameters such as lag-time (λ), specific growth rate (μ), and GFP rate were calculated through linear regression. This analysis was facilitated by the QurvE web tool (Wirth et al., 2023). In some instances, we normalized the data on relative growth rates and GFP rates to make it simpler to compare with the control sample.

4.7. Vector construction

Oligonucleotides employed in this study are detailed in Supplementary Table 1. We sourced these oligonucleotides from Integrated DNA Technologies (Coralville, IA). PrimeSTAR GXL DNA Polymerase (Takara Bio, Shiga, Japan) and Q5 High-Fidelity DNA Polymerase (New England Biolabs) were used for high-fidelity PCR amplifications and genetic analysis. PCR products and plasmids from *E. coli* were purified using the DNA Clean & Concentrator (Zymo Research) and the Monarch Plasmid DNA Miniprep Kit (New England Biolabs), respectively. Plasmid was constructed using the NEBuilder HiFi DNA Assembly Master Mix (New England Biolabs). To facilitate gene deletion, knockout (KO), and plasmids were created to generate transforming DNA (tDNA), in line with methods detailed in a previous study (Shin et al., 2023). Homology arms (HAs) of about 2 Kb adjacent to each target region were amplified from *Vn* genomic DNA, employing specific primers listed in Supplementary Table 1. These HAs, together with the antibiotic resistance cassettes ($Carb^R$ or $Spec^R$), were integrated into the pACYC184 DNA fragment using the NEBuilder HiFi DNA Assembly Master Mix (New England Biolabs), resulting in ptDNA-"Δstrain name" plasmids. The sequence of each tDNA plasmid was confirmed by Sanger sequencing at Eton Bioscience (San Diego, CA). For complementation experiments, each target gene was amplified using primer pairs "KO-strain-name"_fwd and "KO-strain-name"_rev from genomic DNA of *Vn* and then cloned into linearized pUC-SpecR-PRUT (pUC-Sm_PRUT_F2/_R2), resulting in five pUC-SpecR-"KO-strain-name" plasmids.

4.8. Electroporation

Electrocompetent *Vn* cells were prepared following a procedure as previously described (Shin et al., 2023). *Vn* cells were cultured overnight in LBv2 medium at 30 °C with agitation at 180 RPM. The cultures were centrifuged at 5000×*g* for 5 min at 4 °C, washed in LBv2, and inoculated into fresh LBv2 medium at a 1:100 dilution. The culture was grown until an OD_{600} of 0.4 was reached. Afterward, cells were centrifuged and washed twice in cold 1M sorbitol. The final pellet was resuspended in 250 μL of cold 1M sorbitol and divided into 50 μL aliquots. For electroporation, a mixture of 100–200 ng of DNA and the electrocompetent cells was transferred to a 0.2 mm Gene Pulser cuvette (Bio-Rad Laboratories) and electroporated using the Bio-Rad Gene Pulser at 800 V, 25 μF, and 1000 Ω. The cells were then recovered in 1 mL of LBv2 media for 1 h at 30 °C with shaking, plated on LBv2 agar plates with antibiotics, and incubated for at least 12 h at room temperature or 8 h at 30 °C. Similarly, BAC DNA was electroporated into NEB 10-beta electrocompetent *E. coli* cells per the manufacturer's instructions. The cells were recovered in 1 mL of SOC media for 1 h at 37 °C with shaking, then plated on LB agar plates with 12.5 μg/mL chloramphenicol and incubated for at least 8 h at 37 °C.

4.9. DNA assembly in Saccharomyces cerevisiae

We developed the pcBAC15a shuttle vector for DNA assembly in yeast and protein expression in *Vn*, based on the design in the previous study (Jana et al., 2021). This vector includes a Bacterial Artificial Chromosome (BAC), *S. cerevisiae* replication centromere CEN, p15A origin, chloramphenicol resistance, HIS3 marker, and *oriT*, with construction primers listed in Supplementary Table 1. For GFP expression, three vector variants were constructed: pcBAC-Ptac-GFP, pcBAC-P-tet-GFP, and pcBAC-PBAD-GFP, utilizing primers also listed in Supplementary Table 1. On these vectors, GFP expression can be induced by IPTG, anhydrotetracycline, or arabinose. Additionally, we developed two plasmids, pcBAC-tetR-Boost-GFP and pcBAC-araC-Boost-GFP, to investigate the function of booster genetic circuits in *Vn*. The former plasmid, pcBAC-tetR-Boost-GFP, exhibits GFP expression inhibition in the presence of anhydrotetracycline but activation in the absence of an inducer or under IPTG conditions. In contrast, the latter, pcBAC-araC-Boost-GFP, shows GFP expression inhibition with arabinose and activation in the absence of an inducer or with IPTG. Following initial experimentation, pcBAC-araC-Boost-GFP was chosen to advance the development of the Acetate Boost Module. To integrate the Acetate

Boost Module in the *Vn* genome, we assembled two shuttle vectors containing the modules. DNA fragments with 60–70 bp homologies, as detailed in Supplementary Table 1, were transformed and assembled in *Saccharomyces cerevisiae* VL6-48 using the LiAc/SS carrier DNA/PEG method (Gietz and Schiestl, 2007). Yeast clones harboring accurately assembled BACs were identified through colony PCR targeting the junctions of the constructs. The BACs were extracted using the Gentra Puregene Yeast/Bact. Kit (Qiagen) from validated yeast clones and electroporated into *E. coli* NEB 10-beta cells. Post-purification in *E. coli*, the sequence of BACs was further verified by the Whole Plasmid Sequencing service in Plasmidsaurus (Eugene, OR).

4.10. Genome editing via natural transformation

To delete genes or insert genetic modules into the genome precisely, we prepared the transforming DNA (tDNA) for natural competence, as previously described (Shin et al., 2023). For gene deletion, tDNA was PCR-amplified using the "*Δstrain name*"_Left_For/Right_Rev primer pair and corresponding knockout (KO) plasmids as templates, as detailed in Supplementary Table 1. The PCR products were treated with DpnI enzyme (New England Biolabs) and purified using the DNA Clean & Concentrator kit (Zymo Research). To insert the Acetate iModulon Boost Module into the genome, we amplified tDNA with Ace2_tDNA_F and Ace2_tDNA_R primer sets, using pcAceiMBoost-A-REV and pcAceiMBoost-B-REV, respectively. The amplified tDNA was further purified from agarose gels using the Zymoclean Gel DNA Recovery Kit (Zymo Research). Natural transformation assays followed the method previously described (Shin et al., 2023). For gene deletion experiments, the Vn-PTrc-TfoX strain (wild-type with pTrc-tfoX plasmid) was used, while ΔArabinose-PTrc-TfoX (ΔArabinose strain with pTrc-tfoX plasmid) was used for constructing AceiMBoost strains. To activate natural competence, these strains carrying the pTrc-tfoX plasmid (inducing *tfoX* expression under the Trc promoter with isopropyl ß-D-1-thiogalactopyranoside (IPTG)) were grown overnight in LBv2 media supplemented with 10 μg/mL Cm and 100 μM IPTG. The cell culture's OD_{600} was adjusted to 4.0, and 5 μL of this culture was transferred to 350 μL of competence buffer (28 g/L Instant Ocean Sea Salt) with 500 μM IPTG. 50 ng of tDNA was added to the cells and mixed gently. The mixtures were incubated at 30 °C for 4 h without shaking, then recovered in 1 mL of fresh LBv2 for 2 h at 30 °C. The cells were then plated on selective agar plates (LBv2 with 50 μg/mL Carb or 360 μg/mL Spec). Gene deletion (Supplementary Fig. 3c) and target DNA integration (Supplementary Fig. 8g) were verified by PCR using genomic DNA and primer set "*Δstrain-name*"_Val_For/Rev or AceiMBoost_Left/Right_Val_For/Rev (for left and right junction) and BoostSm_For/-BoostPBAD_For (for internal region), as listed in Supplementary Table 1.

4.11. Statistical analysis

Beyond transcriptomic analysis and ICA, further statistical evaluations were conducted using GraphPad Prism v10 software (GraphPad, San Diego, CA, USA). These included Pearson's correlation coefficient, the two-tailed Student's t-test, and the two-tailed Wilcoxon-Mann-Whitney test. Statistical significance was established at *P*-values less than 0.05.

CRediT authorship contribution statement

Jongoh Shin: Writing – review & editing, Writing – original draft, Validation, Methodology, Investigation, Formal analysis, Data curation, Conceptualization. **Daniel C. Zielinski:** Writing – review & editing, Writing – original draft, Investigation. **Bernhard O. Palsson:** Writing – review & editing, Writing – original draft, Supervision, Project administration, Investigation, Funding acquisition, Conceptualization.

Declaration of competing interest

The authors have no competing interests to declare.

Data availability

All RNA-Seq data and iModulon information are publicly available

Acknowledgment

We would like to thank Marc Abrams (Systems Biology Research Group, University of California San Diego) for assistance with paper editing. This work was supported by The Novo Nordisk Foundation (NNF) Center for Biosustainability (CfB) at the Technical University of Denmark (NNF20CC0035580) and the Y.C. Fung Endowed Chair in Bioengineering at the University of California San Diego.

Appendix A. Supplementary data

Supplementary data to this article can be found online at https://doi.org/10.1016/j.ymben.2024.05.007.

References

Anand, A., Chen, K., Catoiu, E., Sastry, A.V., Olson, C.A., Sandberg, T.E., Seif, Y., Xu, S., Szubin, R., Yang, L., Feist, A.M., Palsson, B.O., 2020. OxyR is a convergent target for mutations acquired during adaptation to oxidative stress-prone metabolic states. Mol. Biol. Evol. 37, 660–667. https://doi.org/10.1093/molbev/msz251.

Asha, R., Niyonzima, F.N., Sunil, S.M., 2013. Purification and properties of pullulanase from Bacillus halodurans. Int. Res. J. Biol. Sci. 2, 35–43.

Bajic, D., Sanchez, A., 2020. The ecology and evolution of microbial metabolic strategies. Curr. Opin. Biotechnol. 62, 123–128. https://doi.org/10.1016/j.copbio.2019.09.003.

Balakrishnan, R., de Silva, R.T., Hwa, T., Cremer, J., 2021. Suboptimal resource allocation in changing environments constrains response and growth in bacteria. Mol. Syst. Biol. 17, e10597 https://doi.org/10.15252/msb.202110597.

Barrett, T., Troup, D.B., Wilhite, S.E., Ledoux, P., Evangelista, C., Kim, I.F., Tomashevsky, M., Marshall, K.A., Phillippy, K.H., Sherman, P.M., Muertter, R.N., Holko, M., Ayanbule, O., Yefanov, A., Soboleva, A., 2011. NCBI GEO: archive for functional genomics data sets–10 years on. Nucleic Acids Res. 39, D1005–D1010. https://doi.org/10.1093/nar/gkq1184.

Basan, M., Honda, T., Christodoulou, D., Hörl, M., Chang, Y.-F., Leoncini, E., Mukherjee, A., Okano, H., Taylor, B.R., Silverman, J.M., Sanchez, C., Williamson, J. R., Paulsson, J., Hwa, T., Sauer, U., 2020. A universal trade-off between growth and lag in fluctuating environments. Nature 584, 470–474. https://doi.org/10.1038/s41586-020-2505-4.

Bentley, G.J., Narayanan, N., Jha, R.K., Salvachúa, D., Elmore, J.R., Peabody, G.L., Black, B.A., Ramirez, K., De Capite, A., Michener, W.E., Werner, A.Z., Klingeman, D. M., Schindel, H.S., Nelson, R., Foust, L., Guss, A.M., Dale, T., Johnson, C.W., Beckham, G.T., 2020. Engineering glucose metabolism for enhanced muconic acid production in Pseudomonas putida KT2440. Metab. Eng. 59, 64–75. https://doi.org/10.1016/j.ymben.2020.01.001.

Bertoldo, C., Duffner, F., Jorgensen, P.L., Antranikian, G., 1999. Pullulanase type I from Fervidobacterium pennavorans Ven5: cloning, sequencing, and expression of the gene and biochemical characterization of the recombinant enzyme. Appl. Environ. Microbiol. 65, 2084–2091. https://doi.org/10.1128/AEM.65.5.2084-2091.1999.

Bosdriesz, E., Molenaar, D., Teusink, B., Bruggeman, F.J., 2015. How fast-growing bacteria robustly tune their ribosome concentration to approximate growth-rate maximization. FEBS J. 282, 2029–2044. https://doi.org/10.1111/febs.13258.

Carey, J.N., Mettert, E.L., Fishman-Engel, D.R., Roggiani, M., Kiley, P.J., Goulian, M., 2019. Phage integration alters the respiratory strategy of its host. Elife 8. https://doi.org/10.7554/eLife.49081.

Chang, D.E., Shin, S., Rhee, J.S., Pan, J.G., 1999. Acetate metabolism in a pta mutant of Escherichia coli W3110: importance of maintaining acetyl coenzyme A flux for growth and survival. J. Bacteriol. 181, 6656–6663. https://doi.org/10.1128/JB.181.21.6656-6663.1999.

Choe, D., Szubin, R., Poudel, S., Sastry, A., Song, Y., Lee, Y., Cho, S., Palsson, B., Cho, B.-K., 2021. RiboRid: a low cost, advanced, and ultra-efficient method to remove ribosomal RNA for bacterial transcriptomics. PLoS Genet. 17, e1009821 https://doi.org/10.1371/journal.pgen.1009821.

Choudhary, K.S., Kleinmanns, J.A., Decker, K., Sastry, A.V., Gao, Y., Szubin, R., Seif, Y., Palsson, B.O., 2020. Elucidation of regulatory modes for five two-component systems in Escherichia coli reveals novel relationships. mSystems 5. https://doi.org/10.1128/mSystems.00980-20.

Coppens, L., Tschirhart, T., Leary, D.H., Colston, S.M., Compton, J.R., Hervey 4th, W.J., Dana, K.L., Vora, G.J., Bordel, S., Ledesma-Amaro, R., 2023. Vibrio natriegens genome-scale modeling reveals insights into halophilic adaptations and resource allocation. Mol. Syst. Biol., e10523 https://doi.org/10.15252/msb.202110523.

Croucher, N.J., Fookes, M.C., Perkins, T.T., Turner, D.J., Marguerat, S.B., Keane, T., Quail, M.A., He, M., Assefa, S., Bähler, J., Kingsley, R.A., Parkhill, J., Bentley, S.D., Dougan, G., Thomson, N.R., 2009. A simple method for directional transcriptome sequencing using Illumina technology. Nucleic Acids Res. 37, e148. https://doi.org/10.1093/nar/gkp811.

Croucher, N.J., Thomson, N.R., 2010. Studying bacterial transcriptomes using RNA-seq. Curr. Opin. Microbiol. 13, 619–624. https://doi.org/10.1016/j.mib.2010.09.009.

Dawan, J., Ahn, J., 2022. Bacterial stress responses as potential targets in overcoming antibiotic resistance. Microorganisms 10. https://doi.org/10.3390/microorganisms10071385.

Derdouri, N., Ginet, N., Denis, Y., Ansaldi, M., Battesti, A., 2023. The prophage-encoded transcriptional regulator AppY has pleiotropic effects on E. coli physiology. PLoS Genet. 19, e1010672 https://doi.org/10.1371/journal.pgen.1010672.

Eagon, R.G., 1962. Pseudomonas natriegens, a marine bacterium with a generation time of less than 10 minutes. J. Bacteriol. 83, 736–737. https://doi.org/10.1128/jb.83.4.736-737.1962.

Eisenreich, W., Dandekar, T., Heesemann, J., Goebel, W., 2010. Carbon metabolism of intracellular bacterial pathogens and possible links to virulence. Nat. Rev. Microbiol. 8, 401–412. https://doi.org/10.1038/nrmicro2351.

Erickson, D.W., Schink, S.J., Patsalo, V., Williamson, J.R., Gerland, U., Hwa, T., 2017. A global resource allocation strategy governs growth transition kinetics of Escherichia coli. Nature 551, 119–123. https://doi.org/10.1038/nature24299.

Ester, Kriegel, Sander, Xu, 1996. A Density-Based Algorithm for Discovering Clusters in Large Spatial Databases with Noise. KDD.

Ewels, P., Magnusson, M., Lundin, S., Käller, M., 2016. MultiQC: summarize analysis results for multiple tools and samples in a single report. Bioinformatics 32, 3047–3048. https://doi.org/10.1093/bioinformatics/btw354.

Fang, F.C., Frawley, E.R., Tapscott, T., Vázquez-Torres, A., 2016. Bacterial stress responses during host infection. Cell Host Microbe 20, 133–143. https://doi.org/10.1016/j.chom.2016.07.009.

Farmer, W.R., Liao, J.C., 1997. Reduction of aerobic acetate production by Escherichia coli. Appl. Environ. Microbiol. 63, 3205–3210. https://doi.org/10.1128/aem.63.8.3205-3210.1997.

Ferreira, F.M., Mendoza-Hernandez, G., Castañeda-Bueno, M., Aparicio, R., Fischer, H., Calcagno, M.L., Oliva, G., 2006. Structural analysis of N-acetylglucosamine-6-phosphate deacetylase apoenzyme from Escherichia coli. J. Mol. Biol. 359, 308–321. https://doi.org/10.1016/j.jmb.2006.03.024.

Gene Ontology Consortium, 2021. The Gene Ontology resource: enriching a GOld mine. Nucleic Acids Res. 49, D325–D334. https://doi.org/10.1093/nar/gkaa1113.

Gietz, R.D., Schiestl, R.H., 2007. High-efficiency yeast transformation using the LiAc/SS carrier DNA/PEG method. Nat. Protoc. 2, 31–34. https://doi.org/10.1038/nprot.2007.13.

Harty, C.E., Martins, D., Doing, G., Mould, D.L., Clay, M.E., Occhipinti, P., Nguyen, D., Hogan, D.A., 2019. Ethanol stimulates trehalose production through a SpoT-DksA-AlgU-dependent pathway in Pseudomonas aeruginosa. J. Bacteriol. 201 https://doi.org/10.1128/JB.00794-18.

Herrou, J., Bompard, C., Antoine, R., Leroy, A., Rucktooa, P., Hot, D., Huvent, I., Locht, C., Villeret, V., Jacob-Dubuisson, F., 2007. Structure-based mechanism of ligand binding for periplasmic solute-binding protein of the Bug family. J. Mol. Biol. 373, 954–964. https://doi.org/10.1016/j.jmb.2007.08.006.

Hidalgo, D., Martínez-Ortiz, C.A., Palsson, B.O., Jiménez, J.I., Utrilla, J., 2022. Regulatory perturbations of ribosome allocation in bacteria reshape the growth proteome with a trade-off in adaptation capacity. iScience 25, 103879. https://doi.org/10.1016/j.isci.2022.103879.

Hoffart, E., Grenz, S., Lange, J., Nitschel, R., Müller, F., Schwentner, A., Feith, A., Lenfers-Lücker, M., Takors, R., Blombach, B., 2017. High substrate uptake rates empower Vibrio natriegens as production host for industrial biotechnology. Appl. Environ. Microbiol. 83, e01614 https://doi.org/10.1128/AEM.01614-17, 17.

Huerta-Cepas, J., Szklarczyk, D., Heller, D., Hernández-Plaza, A., Forslund, S.K., Cook, H., Mende, D.R., Letunic, I., Rattei, T., Jensen, L.J., von Mering, C., Bork, P., 2019. eggNOG 5.0: a hierarchical, functionally and phylogenetically annotated orthology resource based on 5090 organisms and 2502 viruses. Nucleic Acids Res. 47, D309–D314. https://doi.org/10.1093/nar/gky1085.

Hyvärinen, A., 1999. Fast and robust fixed-point algorithms for independent component analysis. IEEE Trans. Neural Network. 10, 626–634. https://doi.org/10.1109/72.761722.

Irving, S.E., Choudhury, N.R., Corrigan, R.M., 2021. The stringent response and physiological roles of (pp)pGpp in bacteria. Nat. Rev. Microbiol. 19, 256–271. https://doi.org/10.1038/s41579-020-00470-y.

Jana, B., Keppel, K., Salomon, D., 2021. Engineering a customizable antibacterial T6SS-based platform in Vibrio natriegens. EMBO Rep. 22, e53681 https://doi.org/10.15252/embr.202153681.

Jozefczuk, S., Klie, S., Catchpole, G., Szymanski, J., Cuadros-Inostroza, A., Steinhauser, D., Selbig, J., Willmitzer, L., 2010. Metabolomic and transcriptomic stress response of Escherichia coli. Mol. Syst. Biol. 6, 364. https://doi.org/10.1038/msb.2010.18.

Kanehisa, M., Furumichi, M., Tanabe, M., Sato, Y., Morishima, K., 2017. KEGG: new perspectives on genomes, pathways, diseases and drugs. Nucleic Acids Res. 45, D353–D361. https://doi.org/10.1093/nar/gkw1092.

Karp, P.D., Billington, R., Caspi, R., Fulcher, C.A., Latendresse, M., Kothari, A., Keseler, I. M., Krummenacker, M., Midford, P.E., Ong, Q., Ong, W.K., Paley, S.M., Subhraveti, P., 2019. The BioCyc collection of microbial genomes and metabolic pathways. Briefings Bioinf. 20, 1085–1093. https://doi.org/10.1093/bib/bbx085.

Kolb, A., Busby, S., Buc, H., Garges, S., Adhya, S., 1993. Transcriptional regulation by cAMP and its receptor protein. Annu. Rev. Biochem. 62, 749–795. https://doi.org/10.1146/annurev.bi.62.070193.003533.

Lamoureux, C.R., Decker, K.T., Sastry, A.V., Rychel, K., Gao, Y., McConn, J.L., Zielinski, D.C., Palsson, B.O., 2023. A multi-scale expression and regulation knowledge base for Escherichia coli. Nucleic Acids Res. 51, 10176–10193. https://doi.org/10.1093/nar/gkad750.

Langmead, B., Trapnell, C., Pop, M., Salzberg, S.L., 2009. Ultrafast and memory-efficient alignment of short DNA sequences to the human genome. Genome Biol. 10, R25. https://doi.org/10.1186/gb-2009-10-3-r25.

Lee, H.H., Ostrov, N., Wong, B.G., Gold, M.A., Khalil, A.S., Church, G.M., 2019. Functional genomics of the rapidly replicating bacterium Vibrio natriegens by CRISPRi. Nat. Microbiol. 4, 1105–1113. https://doi.org/10.1038/s41564-019-0423-8.

Leinonen, R., Sugawara, H., Shumway, M., International Nucleotide Sequence Database Collaboration, 2011. The sequence read archive. Nucleic Acids Res. 39, D19–D21. https://doi.org/10.1093/nar/gkq1019.

Liao, Y., Smyth, G.K., Shi, W., 2014. featureCounts: an efficient general purpose program for assigning sequence reads to genomic features. Bioinformatics 30, 923–930. https://doi.org/10.1093/bioinformatics/btt656.

Lim, H.G., Rychel, K., Sastry, A.V., Bentley, G.J., Mueller, J., Schindel, H.S., Larsen, P.E., Laible, P.D., Guss, A.M., Niu, W., Johnson, C.W., Beckham, G.T., Feist, A.M., Palsson, B.O., 2022. Machine-learning from Pseudomonas putida KT2440 transcriptomes reveals its transcriptional regulatory network. Metab. Eng. 72, 297–310. https://doi.org/10.1016/j.ymben.2022.04.004.

Martínez, J.L., Rojo, F., 2011. Metabolic regulation of antibiotic resistance. FEMS Microbiol. Rev. 35, 768–789. https://doi.org/10.1111/j.1574-6976.2011.00282.x.

Martínez-Gómez, K., Flores, N., Castañeda, H.M., Martínez-Batallar, G., Hernández-Chávez, G., Ramírez, O.T., Gosset, G., Encarnación, S., Bolivar, F., 2012. New insights into Escherichia coli metabolism: carbon scavenging, acetate metabolism and carbon recycling responses during growth on glycerol. Microb. Cell Factories 11, 46. https://doi.org/10.1186/1475-2859-11-46.

McConn, J.L., Lamoureux, C.R., Poudel, S., Palsson, B.O., Sastry, A.V., 2021. Optimal dimensionality selection for independent component analysis of transcriptomic data. BMC Bioinf. 22, 584. https://doi.org/10.1186/s12859-021-04497-7.

Miano, A., Rychel, K., Lezia, A., Sastry, A., Palsson, B., Hasty, J., 2023. High-resolution temporal profiling of E. coli transcriptional response. Nat. Commun. 14, 7606. https://doi.org/10.1038/s41467-023-43173-7.

Millard, P., Enjalbert, B., Uttenweiler-Joseph, S., Portais, J.-C., Létisse, F., 2021. Control and regulation of acetate overflow in Escherichia coli. Elife 10. https://doi.org/10.7554/eLife.63661.

Millard, P., Gosselin-Monplaisir, T., Uttenweiler-Joseph, S., Enjalbert, B., 2023. Acetate is a beneficial nutrient for E. coli at low glycolytic flux. EMBO J. 42, e113079 https://doi.org/10.15252/embj.2022113079.

Moritz, B., Striegel, K., de Graaf, A.A., Sahm, H., 2002. Changes of pentose phosphate pathway flux in vivo in Corynebacterium glutamicum during leucine-limited batch cultivation as determined from intracellular metabolite concentration measurements. Metab. Eng. 4, 295–305. https://doi.org/10.1006/mben.2002.0233.

Mulligan, C., Fischer, M., Thomas, G.H., 2011. Tripartite ATP-independent periplasmic (TRAP) transporters in bacteria and archaea. FEMS Microbiol. Rev. 35, 68–86. https://doi.org/10.1111/j.1574-6976.2010.00236.x.

Niehaus, F., Peters, A., Groudieva, T., Antranikian, G., 2000. Cloning, expression and biochemical characterisation of a unique thermostable pullulan-hydrolysing enzyme from the hyperthermophilic archaeon Thermococcus aggregans. FEMS Microbiol. Lett. 190, 223–229. https://doi.org/10.1111/j.1574-6968.2000.tb09290.x.

Nimbalkar, P.R., Khedkar, M.A., Parulekar, R.S., Chandgude, V.K., Sonawane, K.D., Chavan, P.V., Bankar, S.B., 2018. Role of trace elements as cofactor: an efficient strategy toward enhanced biobutanol production. ACS Sustain. Chem. Eng. 6, 9304–9313. https://doi.org/10.1021/acssuschemeng.8b01611.

Nocek, B., Stein, A.J., Jedrzejczak, R., Cuff, M.E., Li, H., Volkart, L., Joachimiak, A., 2011. Structural studies of ROK fructokinase YdhR from Bacillus subtilis: insights into substrate binding and fructose specificity. J. Mol. Biol. 406, 325–342. https://doi.org/10.1016/j.jmb.2010.12.021.

Oliver, J.D., 2010. Recent findings on the viable but nonculturable state in pathogenic bacteria. FEMS Microbiol. Rev. 34, 415–425. https://doi.org/10.1111/j.1574-6976.2009.00200.x.

Osman, D., Foster, A.W., Chen, J., Svedaite, K., Steed, J.W., Lurie-Luke, E., Huggins, T.G., Robinson, N.J., 2017. Fine control of metal concentrations is necessary for cells to discern zinc from cobalt. Nat. Commun. 8, 1884. https://doi.org/10.1038/s41467-017-02085-z.

Pedregosa, F., Varoquaux, G., Gramfort, A., Michel, V., Thirion, B., Grisel, O., Blondel, M., Prettenhofer, P., Weiss, R., Dubourg, V., Vanderplas, J., Passos, A., Cournapeau, D., Brucher, M., Perrot, M., Duchesnay, É., 2011. Scikit-learn: machine learning in Python. J. Mach. Learn. Res. 12, 2825–2830.

Pinhal, S., Ropers, D., Geiselmann, J., de Jong, H., 2019. Acetate metabolism and the inhibition of bacterial growth by acetate. J. Bacteriol. 201 https://doi.org/10.1128/JB.00147-19.

Poudel, S., Tsunemoto, H., Seif, Y., Sastry, A.V., Szubin, R., Xu, S., Machado, H., Olson, C. A., Anand, A., Pogliano, J., Nizet, V., Palsson, B.O., 2020. Revealing 29 sets of independently modulated genes in *Staphylococcus aureus*, their regulators, and role in key physiological response. Proc. Natl. Acad. Sci. USA 117, 17228–17239. https://doi.org/10.1073/pnas.2008413117.

Rajput, A., Tsunemoto, H., Sastry, A.V., Szubin, R., Rychel, K., Chauhan, S.M., Pogliano, J., Palsson, B.O., 2022. Advanced transcriptomic analysis reveals the role of efflux pumps and media composition in antibiotic responses of Pseudomonas aeruginosa. Nucleic Acids Res. 50, 9675–9688. https://doi.org/10.1093/nar/gkac743.

Rosa, L.T., Bianconi, M.E., Thomas, G.H., Kelly, D.J., 2018. Tripartite ATP-independent periplasmic (TRAP) transporters and tripartite tricarboxylate transporters (TTT):

from uptake to pathogenicity. Front. Cell. Infect. Microbiol. 8, 33. https://doi.org/10.3389/fcimb.2018.00033.
Rosano, G.L., Ceccarelli, E.A., 2014. Recombinant protein expression in Escherichia coli: advances and challenges. Front. Microbiol. 5, 172. https://doi.org/10.3389/fmicb.2014.00172.
Roszak, D.B., Colwell, R.R., 1987. Survival strategies of bacteria in the natural environment. Microbiol. Rev. 51, 365–379. https://doi.org/10.1128/mr.51.3.365-379.1987.
Rucktooa, P., Antoine, R., Herrou, J., Huvent, I., Locht, C., Jacob-Dubuisson, F., Villeret, V., Bompard, C., 2007. Crystal structures of two Bordetella pertussis periplasmic receptors contribute to defining a novel pyroglutamic acid binding DctP subfamily. J. Mol. Biol. 370, 93–106. https://doi.org/10.1016/j.jmb.2007.04.047.
Ruzheinikov, S.N., Burke, J., Sedelnikova, S., Baker, P.J., Taylor, R., Bullough, P.A., Muir, N.M., Gore, M.G., Rice, D.W., 2001. Glycerol dehydrogenase. structure, specificity, and mechanism of a family III polyol dehydrogenase. Structure 9, 789–802. https://doi.org/10.1016/s0969-2126(01)00645-1.
Rychel, K., Decker, K., Sastry, A.V., Phaneuf, P.V., Poudel, S., Palsson, B.O., 2021. iModulonDB: a knowledgebase of microbial transcriptional regulation derived from machine learning. Nucleic Acids Res. 49, D112–D120. https://doi.org/10.1093/nar/gkaa810.
Rychel, K., Tan, J., Patel, A., Lamoureux, C., Hefner, Y., Szubin, R., Johnsen, J., Mohamed, E.T.T., Phaneuf, P.V., Anand, A., Olson, C.A., Park, J.H., Sastry, A.V., Yang, L., Feist, A.M., Palsson, B.O., 2023. Laboratory evolution, transcriptomics, and modeling reveal mechanisms of paraquat tolerance. Cell Rep. 42, 113105 https://doi.org/10.1016/j.celrep.2023.113105.
Saelens, W., Cannoodt, R., Saeys, Y., 2018. A comprehensive evaluation of module detection methods for gene expression data. Nat. Commun. 9, 1–12. https://doi.org/10.1038/s41467-018-03424-4.
Sastry, A.V., Dillon, N., Anand, A., Poudel, S., Hefner, Y., Xu, S., Szubin, R., Feist, A.M., Nizet, V., Palsson, B., 2021a. Machine learning of bacterial transcriptomes reveals responses underlying differential antibiotic susceptibility. mSphere 6, e0044321. https://doi.org/10.1128/mSphere.00443-21.
Sastry, A.V., Gao, Y., Szubin, R., Hefner, Y., Xu, S., Kim, D., Choudhary, K.S., Yang, L., King, Z.A., Palsson, B.O., 2019. The Escherichia coli transcriptome mostly consists of independently regulated modules. Nat. Commun. 10, 1–14. https://doi.org/10.1038/s41467-019-13483-w.
Sastry, A.V., Poudel, S., Rychel, K., Yoo, R., Lamoureux, C.R., Chauhan, S., Haiman, Z.B., Al Bulushi, T., Seif, Y., Palsson, B.O., 2021b. Mining all publicly available expression data to compute dynamic microbial transcriptional regulatory networks. bioRxiv. https://doi.org/10.1101/2021.07.01.450581.
Schothorst, J., Zeebroeck, G.V., Thevelein, J.M., 2017. Identification of Ftr1 and Zrt1 as iron and zinc micronutrient transceptors for activation of the PKA pathway in *Saccharomyces cerevisiae*. Microb. Cell Factories 4, 74–89. https://doi.org/10.15698/mic2017.03.561.
Shang, T., Fang, C.M., Ong, C.E., Pan, Y., 2023. Heterologous expression of recombinant human cytochrome P450 (CYP) in Escherichia coli: N-terminal modification, expression, isolation, purification, and reconstitution. BioTech (Basel) 12. https://doi.org/10.3390/biotech12010017.
Shin, J., Rychel, K., Palsson, B.O., 2023. Systems biology of competency in Vibrio natriegens is revealed by applying novel data analytics to the transcriptome. Cell Rep. 42, 112619 https://doi.org/10.1016/j.celrep.2023.112619.
Soini, J., Ukkonen, K., Neubauer, P., 2008. High cell density media for Escherichia coli are generally designed for aerobic cultivations - consequences for large-scale bioprocesses and shake flask cultures. Microb. Cell Factories 7, 26. https://doi.org/10.1186/1475-2859-7-26.
Soma, Y., Tominaga, S., Tokito, K., Imado, Y., Naka, K., Hanai, T., Takahashi, M., Izumi, Y., Bamba, T., 2023. Trace impurities in sodium phosphate influences the physiological activity of Escherichia coli in M9 minimal medium. Sci. Rep. 13, 17396 https://doi.org/10.1038/s41598-023-44526-4.
Stadtman, T.C., 2005. Selenoproteins–tracing the role of a trace element in protein function. PLoS Biol. 3, e421. https://doi.org/10.1371/journal.pbio.0030421.
Sui, Y.-F., Schütze, T., Ouyang, L.-M., Lu, H., Liu, P., Xiao, X., Qi, J., Zhuang, Y.-P., Meyer, V., 2020. Engineering cofactor metabolism for improved protein and glucoamylase production in Aspergillus Niger. Microb. Cell Factories 19, 198. https://doi.org/10.1186/s12934-020-01450-w.
Thoma, F., Blombach, B., 2021. Metabolic engineering of Vibrio natriegens. Essays Biochem. 65, 381–392. https://doi.org/10.1042/EBC20200135.
Tian, J., Deng, W., Zhang, Z., Xu, J., Yang, G., Zhao, G., Yang, S., Jiang, W., Gu, Y., 2023. Discovery and remodeling of Vibrio natriegens as a microbial platform for efficient formic acid biorefinery. Nat. Commun. 14, 7758. https://doi.org/10.1038/s41467-023-43631-2.
UniProt Consortium, 2021. UniProt: the universal protein knowledgebase in 2021. Nucleic Acids Res. 49, D480–D489. https://doi.org/10.1093/nar/gkaa1100.
Voth, W., Jakob, U., 2017. Stress-activated chaperones: a first line of defense. Trends Biochem. Sci. 42, 899–913. https://doi.org/10.1016/j.tibs.2017.08.006.
Wang, J.D., Levin, P.A., 2009. Metabolism, cell growth and the bacterial cell cycle. Nat. Rev. Microbiol. 7, 822–827. https://doi.org/10.1038/nrmicro2202.
Wang, L., Wang, S., Li, W., 2012. RSeQC: quality control of RNA-seq experiments. Bioinformatics 28, 2184–2185. https://doi.org/10.1093/bioinformatics/bts356.
Wangpaiboon, K., Charoenwongpaiboon, T., Klaewkla, M., Field, R.A., Panpetch, P., 2023. Cassava pullulanase and its synergistic debranching action with isoamylase 3 in starch catabolism. Front. Plant Sci. 14, 1114215 https://doi.org/10.3389/fpls.2023.1114215.
Wei, W., Ma, J., Chen, S.-Q., Cai, X.-H., Wei, D.-Z., 2015. A novel cold-adapted type I pullulanase of Paenibacillus polymyxa Nws-pp2: in vivo functional expression and biochemical characterization of glucans hydrolyzates analysis. BMC Biotechnol. 15, 96. https://doi.org/10.1186/s12896-015-0215-z.
Weinstock, M.T., Hesek, E.D., Wilson, C.M., Gibson, D.G., 2016. Vibrio natriegens as a fast-growing host for molecular biology. Nat. Methods 13, 849–851. https://doi.org/10.1038/nmeth.3970.
Wirth, N.T., Funk, J., Donati, S., Nikel, P.I., 2023. QurvE: user-friendly software for the analysis of biological growth and fluorescence data. Nat. Protoc. 18, 2401–2403. https://doi.org/10.1038/s41596-023-00850-7.
Wolfe, Alan J., 2005. The acetate switch. Microbiol. Mol. Biol. Rev. 69, 12–50. https://doi.org/10.1128/mmbr.69.1.12-50.2005.
Xu, J., Dong, F., Wu, Meixian, Tao, R., Yang, J., Wu, Mianbin, Jiang, Y., Yang, S., Yang, L., 2021. Vibrio natriegens as a pET-compatible expression host complementary to Escherichia coli. Front. Microbiol. 12, 627181 https://doi.org/10.3389/fmicb.2021.627181.
You, C., Okano, H., Hui, S., Zhang, Z., Kim, M., Gunderson, C.W., Wang, Y.-P., Lenz, P., Yan, D., Hwa, T., 2013. Coordination of bacterial proteome with metabolism by cyclic AMP signalling. Nature 500, 301–306. https://doi.org/10.1038/nature12446.
Zhu, M., Dai, X., 2023. Stringent response ensures the timely adaptation of bacterial growth to nutrient downshift. Nat. Commun. 14, 467. https://doi.org/10.1038/s41467-023-36254-0.